Remarks on worldsheet theories dual to free large N gauge theories

Ofer Aharony,[1,2] Justin R. David,[3] Rajesh Gopakumar,[3] Zohar Komargodski,[1] and Shlomo S. Razamat[4]

[1]*Department of Particle Physics, Weizmann Institute of Science, Rehovot 76100, Israel*
[2]*SITP, Department of Physics and SLAC, Stanford University, Stanford, California 94305, USA*
[3]*Harish-Chandra Research Institute, Chhatnag Road, Jhunsi, Allahabad 211019, India*
[4]*Department of Physics, Technion, Israel Institute of Technology, Haifa 32000, Israel*

(Received 26 March 2007; published 30 May 2007)

We continue to investigate properties of the worldsheet conformal field theories (CFTs) which are conjectured to be dual to free large N gauge theories, using the mapping of Feynman diagrams to the worldsheet suggested in [R. Gopakumar, Phys. Rev. D **70**, 025009 (2004); **70**, 025010 (2004); C. R. Physique **5**, 1111 (2004); Phys. Rev. D **72**, 066008 (2005)]. The modular invariance of these CFTs is shown to be built into the formalism. We show that correlation functions in these CFTs which are localized on subspaces of the moduli space may be interpreted as delta-function distributions, and that this can be consistent with a local worldsheet description given some constraints on the operator product expansion coefficients. We illustrate these features by a detailed analysis of a specific four-point function diagram. To reliably compute this correlator, we use a novel perturbation scheme which involves an expansion in the large dimension of some operators.

DOI: 10.1103/PhysRevD.75.106006 PACS numbers: 11.25.Mj, 11.15.Pg, 11.25.Tq

I. INTRODUCTION

Since the seminal work of 't Hooft [1], it has been widely believed that large N $SU(N)$ gauge theories (with adjoint matter fields) should have a dual description in terms of closed strings with a string coupling constant $g_s \sim 1/N$. The original argument for this duality was based on the reinterpretation of Feynman diagrams as string theory diagrams. Feynman diagrams drawn in 't Hooft's double-line notation resemble two-dimensional surfaces with holes. It was conjectured that there should be an equivalent description in which the holes get filled up, leading to closed Riemann surfaces without boundaries.

The arguments of 't Hooft do not give a prescription to construct the string theory dual to a specific large N gauge theory. Numerous attempts have been made to directly construct string theory duals for given field theories. However, success was mainly achieved when the field theory had a topological interpretation (Chern-Simons theory [2] and the Kontsevich model [3] are good examples of this) or the putative dual string theory was exactly solvable ($d \leq 2$ string/matrix model duality). This situation has changed following the AdS/CFT correspondence [4]. By now, there are many examples in which it is known how to find the closed string dual of gauge theories which can be realized as the world-volume theories of D-branes in some decoupling limit. In these cases the closed string dual turns out to be a standard closed string theory, living in a warped higher dimensional space. In some cases, for which the gauge theory is strongly coupled, the dual string background is weakly curved and a gravity approximation of the string theory may be used. In general (and, in particular, for all weakly coupled gauge theories), this is not the case, and the dual string theory is complicated (and does not necessarily have a geometrical interpretation).

It is interesting to ask what is the string theory dual of the simplest large N gauge theory, the free gauge theory.[1] There have been various proposals for how to study the string dual of free large N gauge theories (see, for instance, [5–14]). It is clear that the dual string theories must live in a highly curved background, which may or may not have a geometrical interpretation (for four-dimensional free gauge theories with massless matter fields, which are conformally invariant, one expects that any geometrical interpretation should include an AdS_5 factor).

In this paper we continue our study of a specific proposal [5][2] for how to map the Feynman diagrams to worldsheets. This proposal is based on rewriting the propagators in the Feynman diagrams as integrals over Schwinger parameters, and mapping these parameters to the moduli of a Riemann surface with holes (which include the moduli of the closed Riemann surface and the circumferences of the holes).[3] One can then integrate over the parameters of the holes, and translate any Feynman diagram to a correlation function on the closed string worldsheet. This proposal makes the procedure advocated by 't Hooft manifest. Most of our discussion will be general, but whenever we need a concrete example we will consider operators involving adjoint scalar fields in a four-dimensional gauge theory.

The mapping of [5] gives a closed string theory whose integrated correlation functions (of physical vertex opera-

[1]Note that the free limit of an $SU(N)$ gauge theory is not the same as a theory of $(N^2 - 1)$ free fields, since the Gauss law constraint is still imposed on physical states. Equivalently, we only consider gauge-invariant operators.

[2]See [15–18] for further work on this proposal.

[3]The holes here are not those of the gauge theory Feynman diagram but rather of its dual. They are therefore as many in number as the vertices of the original graph.

tors), by construction, reproduce the space-time correlation functions. The worldsheet theory is also automatically conformally invariant (so that it can be interpreted as a closed string theory in conformal gauge) and modular invariant. However, the construction does not give a Lagrangian for the worldsheet theory, and it is not clear from the construction if this worldsheet theory is a standard local conformal field theory or not.

It was noted in [16] that the prescription of [5] gives rise to an interesting feature, which naively is in contradiction to having a well-behaved worldsheet field theory: some of the putative worldsheet correlators localize on lower-dimension subspaces of the moduli space of marked Riemann surfaces. In a usual local field theory, one expects the worldsheet correlator to be a smooth function on the moduli space, which naively rules out any localization on subspaces. In this paper we claim that such a localization can arise in specific field theories by a special conspiracy between the operator product expansion (OPE) coefficients. We also discuss the manifestation of modular invariance in the prescription of [5]. Although modular invariance is guaranteed by the prescription, we will illustrate that in some amplitudes it is realized in a quite intricate manner.

This paper is organized as follows. In Sec. II we present the problems of modular invariance and the localization on the worldsheet and our suggested resolution of these problems. In Sec. III we concentrate on a specific four-point function: the ''Broom'' diagram. This diagram does not localize on a subspace of the moduli space, but it has limits in which it goes over to a localized diagram. We discuss the limits in which this diagram can illustrate different general features of the prescription, and we perform an explicit perturbative analysis of the diagram around exactly solvable limits. In Sec. IV we present results about more general exactly solvable subspaces of the Broom diagram, which serve as a check on the perturbative analysis. In Sec. V we discuss the delocalization of the worldsheet amplitudes as illustrated by the field theory analysis of Broom correlators. We end in Sec. VI with a summary and a discussion of some open problems. In Appendix A we discuss the elliptic function approach to the Strebel problem which arises in computing the Broom diagram in more detail, and present the matching between perturbation theory and the exact results. In Appendix B two other diagrams which also localize on a subspace of the moduli space, the Square diagram and the Whale diagram, are analyzed. We show that the Whale diagram localizes in a different way than the other diagrams we discuss: it localizes on a two-dimensional subspace of the two-dimensional moduli space.

II. GENERAL FEATURES

In [5] a specific prescription was suggested for mapping the correlation functions of free large N gauge theories to a string worldsheet, in the 't Hooft large N limit [1]. This prescription involves rewriting each Feynman diagram contributing to an n-point correlation function as an integral over the Schwinger parameters of the propagators, after reduction to a ''skeleton graph'' in which homotopically equivalent propagators (when the Feynman diagram is interpreted as a genus g Riemann surface using the double-line notation) are joined together, and then mapping the space of these Schwinger parameters to the ''decorated moduli space'' $\mathcal{M}_{g,n} \times \mathbb{R}_+^n$. This is the moduli space of genus g Riemann surfaces with n marked points, together with a positive number p_i associated with each point. As described in detail in [5], this mapping uses the properties of Strebel differentials[4] on genus g Riemann surfaces. After integrating over the p_i, this procedure gives a specific worldsheet n-point correlation function associated with this Feynman diagram which, by construction, reproduces the correct n-point space-time correlation function (upon integration over the worldsheet moduli).

Certain properties of the mapping proposed in [5] and of the worldsheet correlation functions it leads to can be understood by general considerations. Two of these properties—the lack of special conformal invariance in space-time and the localization of certain amplitudes on lower-dimension subspaces of the moduli space—were elucidated in [16]. We begin this section by discussing another general property of the resulting worldsheet correlation functions, which is modular invariance. We then discuss in more detail the interpretation of the amplitudes which are localized on the moduli space. We argue that these amplitudes should be interpreted as delta-function distributions, and we discuss why the appearance of such distributions in correlation functions is not necessarily in contradiction with a local worldsheet interpretation. In fact, we derive some general constraints on the OPE coefficients of the putative local worldsheet theory which are needed for reproducing the localized correlation function.

In order to establish an exact sense in which the localized correlators should be treated as delta functions, we analyze a small deformation of the localized diagram. This deformation involves taking the limit of correlation functions with a large number of field contractions between the vertex operators of the original localized diagram, and a small number of additional contractions. We argue that such correlation functions are smooth but tend to localize near subspaces of the moduli space, and that the mapping (and the corresponding Strebel differentials) may be computed perturbatively in the inverse number of fields (or in the distance from the localized limit). By using this expansion we can show that in the limit in which the correlation functions localize they become delta-function distributions.

[4]See [19–21] for details about Strebel differentials and [22–24] for additional applications of these differentials in string theory.

In the subsequent sections of the paper, we discuss in detail a particular 4-point function diagram, which we call the Broom diagram, and we use this diagram to illustrate the general features described in this section. In particular, the expansion method described in Sec. II B may be used to compute this diagram in some regions of its parameters.

A. Modular invariance of worldsheet amplitudes defined by the procedure of [5]

In this subsection we discuss how modular invariance is realized in the prescription suggested in [5]. The mapping from the Schwinger parameters on the gauge theory side to the decorated moduli space of the Riemann surfaces $\mathcal{M}_{g,n} \times \mathbb{R}_+^n$ is, by construction, consistent with the action of the modular group on this space. The mapping uses the Strebel theorem to relate the two, which ensures that (for generic Feynman diagrams) we cover the whole decorated moduli space (after the identifications imposed by the modular group) and we cover it exactly once.

However, the way that modular invariance is technically realized can in some cases be nontrivial. This is because the mapping of [5] involves taking the square root of the Strebel differential. In cases where this square root has branch cuts, one must be careful to choose specific branches in order to ensure that the final worldsheet correlators are single valued on the moduli space.

Several correlators were analyzed in [16,17], where it was shown by direct computation that these amplitudes are consistent with the modular invariance. However, in all of these cases the square roots of the Strebel differentials corresponding to the diagrams contributing to those amplitudes did not include fractional powers and thus did not have any branch cuts. In this paper we will analyze in detail a diagram which does have branch cuts for the square root of the Strebel differential. Note that the existence of the branch cuts does not affect "large modular transformations" such as $\eta \to 1/\eta$, but periodicity issues, such as taking two points in a closed path around each other or taking the torus modular parameter τ to $\tau + 1$, should be addressed with more care. We will illustrate the general issue in this subsection by looking at general properties of 4-point functions on the sphere. A specific example will be discussed in the next section.

Consider a four-point correlator on the gauge theory side,

$$\langle \mathcal{O}_1(x_1)\mathcal{O}_2(x_2)\mathcal{O}_3(x_3)\mathcal{O}_4(x_4)\rangle. \tag{1}$$

In the suggested mapping, we map the space-time operators $\mathcal{O}_i(x_i)$ to worldsheet operators $V_{i,x_i}(z)$, and we are given a specific procedure to calculate

$$\langle V_{1,x_1}(0)V_{2,x_2}(1)V_{3,x_3}(\eta)V_{4,x_4}(\infty)\rangle. \tag{2}$$

Note that when we write the field theory graph and assign specific operators to each node, this by itself does not fix the assignment of the positions of the dual operators on the worldsheet. The mapping of [5] is modular invariant; however, it is usually convenient to fix the modular freedom by choosing three specific operators to map to three specific locations, as indicated in (2). Of course, we could also choose to fix the modular group in any other way, and all such ways are related by $SL(2,\mathbb{C})$ modular transformations.

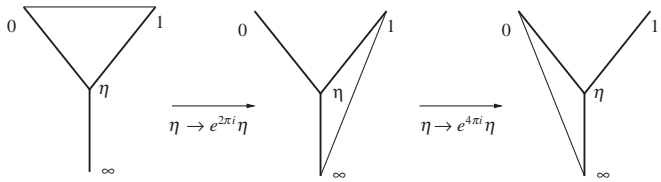

FIG. 1. The skeleton graph which we refer to as the "Broom diagram." We depict here what happens if we make the *naive* choice of branches, in which we do not change branches when we rotate η. We see that for this choice the rotation in the η plane changes the position of one of the edges, and thus changes the correlator we are computing.

Once we choose such a specific fixing of the modular group we can find the correlator (2) using the mapping of [5]. However, when we do this we can find that the relation between the Schwinger parameters and η is such that there are apparently branch cuts on the η-plane. This would lead to an ambiguity in rotating η by a full circle around (say) $z = 0$. Since the mapping of [5] is well defined,[5] it is clear that there exists a choice of the branch which leads to an answer which is single valued, i.e. periodic under a rotation taking $\eta \to e^{2\pi i}\eta$. However, in some cases this choice of branch is not the most natural one, and it requires changing the branch of the square root at some point when we rotate. Obviously, such a change in the branch is only consistent if the correlator vanishes at some point on every path taking $\eta \to e^{2\pi i}\eta$, and this is indeed what we will find in our example in Sec. III A 1.

To illustrate this subtle point consider the "Broom diagram," illustrated in Fig. 1. In this example it turns out, as we will discuss in more detail in Sec. III A 1 below, that if we stay on the same branch of the square root of the Strebel differential, the topology of the critical graph of this differential changes as we take $\eta \to e^{2\pi i}\eta$, leading to a different Feynman diagram, as described in Fig. 1. Thus, one should be careful about the choices of branches when performing computations using the procedure of [5]. However, this subtle issue does not affect the fact that the prescription of [5] always gives modular-invariant answers.

[5]Given a set of Schwinger parameters there is a unique set of circumferences and the position on the moduli space is unique up to the modular group, which we fixed as described above. In other words, the prescription does not distinguish between η and $\eta e^{2\pi i k}$.

B. Short edge expansions

In this subsection we describe a limit of free field theory correlation functions which is governed by a saddle point in the Schwinger parameter space. The expansion in the position of the saddle point corresponds to an expansion in the length of one or more small edges in the critical graph of the corresponding Strebel differential. As we will see in the next subsection, this is useful for analyzing correlators involving diagrams whose contributions are localized on subspaces of the moduli space. These are always diagrams whose dual graph (which is the critical graph of the Strebel differential) has some vanishing edges.

For simplicity, consider a four-dimensional large N gauge theory, and consider a correlation function

$$\left\langle \prod_{i=1}^{n} \mathcal{O}_i(x_i) \right\rangle \tag{3}$$

of gauge-invariant operators made purely of adjoint scalar fields. In the free gauge theory, each Feynman graph corresponding to such a correlation function involves J_{ij} contractions of fields between the ith and the jth operator, so that the answer is given by

$$\prod_{1\le i<j\le n} |x_i - x_j|^{-2J_{ij}}. \tag{4}$$

In the Schwinger parametrization (which generalizes the one used in [5] to position space), this is rewritten as (up to a constant)

$$\int \prod_{1\le i<j\le n, J_{ij}>0} d\sigma_{ij} \sigma_{ij}^{J_{ij}-1} e^{-\sigma_{ij}|x_i-x_j|^2}, \tag{5}$$

and the integration over the σ's is identified with the integral over the decorated moduli space of Riemann surfaces, with the σ's identified with the lengths of the edges of the critical graph of the Strebel differential. When some of the J_{ij} vanish so that some of the σ integrations are not present, this integral is localized on a subspace of the decorated moduli space, and it may also be localized on a subspace of the moduli space, as discussed in [16].

Note that a rescaling of all the σ's acts on the decorated moduli space just by rescaling the p_i's, without changing the position on $\mathcal{M}_{g,n}$. Thus, the position on the moduli space is independent of the overall scale but depends only on the ratios of the σ_{ij}'s. It is then useful to separate the integral into the overall length and the ratios. When (say) $J_{12} > 0$, we can do this by defining $s_{ij} \equiv \sigma_{ij}/\sigma_{12}$. Denoting by S_1 the set $\{(i,j)|1 \le i < j \le n, J_{ij} > 0\}$ and by S_2 the set $S_1 - (1,2)$, we can rewrite (5) as

$$\int d\sigma_{12} \left(\prod_{(i,j)\in S_2} ds_{ij} s_{ij}^{J_{ij}-1} \right) \sigma_{12}^{\Sigma_{(i,j)\in S_1}(J_{ij}-1)} \times e^{-\sigma_{12}(|x_1-x_2|^2 + \Sigma_{(i,j)\in S_2} s_{ij}|x_i-x_j|^2)} \tag{6}$$

or (up to a constant)

$$\int \left(\prod_{(i,j)\in S_2} ds_{ij} s_{ij}^{J_{ij}-1} \right) \times \left(|x_1 - x_2|^2 + \sum_{(i,j)\in S_2} s_{ij}|x_i - x_j|^2 \right)^{-\Sigma_{(i,j)\in S_1}(J_{ij}-1)-1}. \tag{7}$$

In general, the integral (7) is quite complicated when written as an integral over the moduli space. However, if we look at the limit when one (or more) of the J_{ij}'s becomes very large, the integral is dominated by a saddle point in the Schwinger parameter space, and can be evaluated in the saddle point approximation. This saddle point maps onto a point in the decorated moduli space (up to the overall scaling of the p_i), and therefore it is also located at a point in the moduli space. In the limit of large $J \equiv \sum_{(i,j)\in S_1} J_{ij}$, and assuming without loss of generality that J_{12} is of order J in this limit,[6] this saddle point is located at (at leading order in $1/J$)

$$s_{ij} = \frac{(J_{ij}-1)|x_1 - x_2|^2}{J_{12}|x_i - x_j|^2}. \tag{8}$$

If all of the J_{ij}'s become large then this saddle point will map onto a point in the middle of the moduli space. However, if one (or more) of the J_{ij}'s remain finite in the large J limit, then the s_{ij} and therefore the Strebel length l_{ij} of the corresponding edge scales as $1/J$ in the large J limit. Thus, expanding in $1/J$ leads to an expansion in small edges of the Strebel differential.

As an example, we can consider the following operators:

$$\begin{aligned} \mathcal{O}_1(x_1) &= \mathrm{Tr}(\Phi_1^{J_1}(x_1)), \\ \mathcal{O}_2(x_2) &= \mathrm{Tr}(\Phi_2^{J_2}\Phi_3^{j}(x_2)), \\ \mathcal{O}_3(x_3) &= \mathrm{Tr}(\Phi_2^{J_2}\Phi_4^{J_3}(x_3)), \\ \mathcal{O}_4(x_4) &= \mathrm{Tr}(\Phi_3^{j}\Phi_4^{J_3}\Phi_1^{J_1}(x_4)), \end{aligned} \tag{9}$$

where Φ_i are some scalar fields in the adjoint of $U(N)$. In this case the only planar diagram that contributes to

$$\langle \mathcal{O}_1(x_1)\mathcal{O}_2(x_2)\mathcal{O}_3(x_3)\mathcal{O}_4(x_4)\rangle \tag{10}$$

has the skeleton drawn in Fig. 2. We can consider the limit where the J_i become large while j remains finite, so that there are many contractions along the bold lines in Fig. 2 and a few contractions on the thin line. The general arguments above imply that in this limit the diagram will get its dominant contribution from Strebel differentials for which the (dual) edge corresponding to the line between x_2 and x_4 is very small.

The limit where edges of the critical graph of the Strebel differential vanish is the same as the limit where several

[6] At least one of the J_{ij}'s must be of order J in this limit, and we choose the ordering of the points so that it is J_{12}.

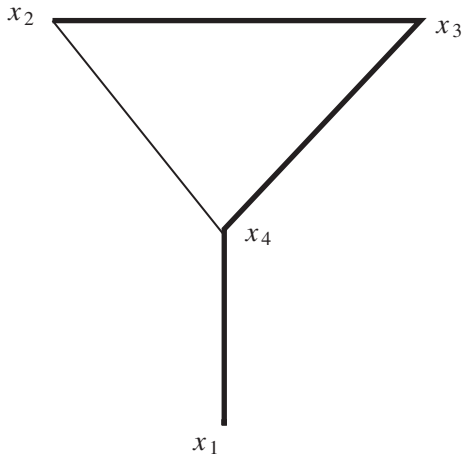

FIG. 2. The skeleton graph of the Broom diagram. The x_i label space-time points where operators are inserted. Bold lines represent many homotopic contractions. On the other hand, the line connecting x_2 and x_4 has a small number of contractions.

zeros of the Strebel differential come together, leading to a nongeneric critical graph. In the limit where the zeros come together, this critical graph is the dual of the field theory diagram which we obtain by removing the edges corresponding to the finite J_{ij}'s from the Feynman graph. Such nongeneric Strebel differentials are often easier to compute. For instance, in the example described above, the differential for the resulting "Π" diagram was computed in [16]. We can then perform a perturbative expansion in the length of the small edges around these nongeneric Strebel differentials, and interpret the result in terms of the large J limit of the field theory correlation functions described above.

In this way, we are able to reliably change variables of integration in some neighborhood of the saddle point of (7). The correlator in the appropriate part of the Riemann surface (which is the image of a neighborhood of the saddle point under the Strebel map) is a very good approximation to the exact result because contributions from other regions in the field theory integral are substantially smaller.

C. Localized correlators as distributions

It was shown in [16] that certain worldsheet correlators, corresponding to nongeneric Feynman diagrams which do not include all possible contractions in their skeleton graph, are localized on lower-dimension subspaces of the moduli space of Riemann surfaces. This localization may perhaps be attributed to the fact that the free field theory is a singular limit from the string theory point of view, which is naively related (at least in the context of string theory on $AdS_5 \times S^5$) to the limit in which the tension of the string vanishes; recall that similar localizations have been encountered also in a different "tensionless" limit [25].[7] So, this fact by itself is not in contradiction with the existence of a local worldsheet description. In this subsection we discuss the interpretation of the localized correlation functions and their implications for the OPE coefficients.

Consider a Feynman diagram giving rise to a localized worldsheet correlator. This correlator may be written as an integral over a subspace of the moduli space of the Riemann surface, which is the subspace spanned by the Strebel differentials whose critical graph has the topology dual to the Feynman graph. This integral, at least in the special case considered above of correlation functions of scalar operators in a four-dimensional gauge theory, is positive definite. This is because the field theory expression for the integral (5) is positive definite, and the mapping of the space of Schwinger parameters to the decorated moduli space is one-to-one (leading to a positive definite Jacobian).

Feynman diagrams with a specific topology for their skeleton graph give localized correlators independently of the number of contractions; in particular, we can consider the limit where the number of contractions J is large. In this limit we can consider adding an additional small number of contractions to the Feynman diagram such that, as described in the previous subsection, they will lead to additional small edges in the critical graph of the Strebel differential, with a length of order $1/J$. Upon adding the additional edges the correlator is no longer localized, and is a smooth function on the moduli space for finite J (this is certainly true if we make all the edges finite, and in many cases it is true even if we just add one small edge). This function is still positive, and in the large J limit it becomes localized on a subspace of the moduli space. Since the localized correlator arises as a limit of smooth positive functions whose integral is finite, it is clear that it must be proportional to a delta-function distribution on the subspace where the correlator is nonvanishing. While our argument that the correlator should be thought of as a delta-function distribution is valid only in the large J limit, it seems likely that the same interpretation of the localized correlators should hold also for finite values of J.

When we have a correlator localized on a lower-dimension subspace of the moduli space, in some cases when we take the OPE limit of two points on the worldsheet approaching each other (say, with two operators at η and at 0 in the $\eta \to 0$ limit), we find that the correlator is localized at a specific angle in the η-plane, for instance that it is nonzero only for (negative) real values of η (as for the Π diagram [16]). How is this consistent with having a smooth OPE? For simplicity let us consider a four-point function which is localized on the negative real axis, namely

$$\langle V_1(\eta)V_2(0)V_3(1)V_4(\infty)\rangle = f(|\eta|)\delta(\theta - \pi) \qquad (11)$$

for some worldsheet operators V_i. Here we have written

[7]Localization of worldsheet correlators on lower-dimension subspaces of the moduli space of Riemann surfaces has also appeared in the framework of string theory in twistor space [26].

$\eta = |\eta| e^{i\theta}$. Let us write the OPE expansion of V_1 and V_2 in the general form

$$V_1(\eta)V_2(0) \simeq \sum_{n,\bar{n}} c_{n\bar{n}}^{12} \mathcal{O}_{n,\bar{n}}(0) \eta^{n-2} \bar{\eta}^{\bar{n}-2}, \tag{12}$$

where the operators $\mathcal{O}_{n,\bar{n}}$ have weight $(n, \bar{n})$ and we assumed that the V_i are physical operators of weight (1, 1). We know from modular invariance that we can limit ourselves to integer spins $n - \bar{n}$, though the sums $n + \bar{n}$ can take any value (and in string duals of conformal field theories it is believed that they take continuous values [16,27]). Combining (11) and (12) and using

$$2\pi\delta(\theta - \pi) = \sum_{k=-\infty}^{\infty} (-1)^k e^{ik\theta}, \tag{13}$$

we obtain that for any given value of $n + \bar{n}$ we must have

$$c_{n\bar{n}}^{12} \langle \mathcal{O}_{n,\bar{n}}(0) V_3(1) V_4(\infty) \rangle \sim \text{constant}_{n+\bar{n}} (-1)^{n-\bar{n}}, \tag{14}$$

where the constant may depend on $n + \bar{n}$ but is independent of $n - \bar{n}$; namely, for every value of $n + \bar{n}$ there must be an infinite series of operators appearing in the OPE, with

$$n = \frac{n+\bar{n}}{2}, \frac{n+\bar{n}}{2} \pm \frac{1}{2}, \frac{n+\bar{n}}{2} \pm 1, \ldots, \tag{15}$$

which all give rise to the same constant in (14). A conspiracy of this form (14) is sufficient for reproducing localized correlation functions of the form (11); any operators appearing in the OPE which are not part of such a conspiracy must not contribute to the localized 4-point functions.

III. THE BROOM DIAGRAM AND ITS LIMITS

In this section we study in detail the Broom diagram and the limits in which it degenerates to the Y and the Π diagrams. In Fig. 3 we have drawn both the field theory diagram and its dual diagram which corresponds to the critical graph of the Strebel differential. The field theory graph is indicated in bolder lines, while the critical graph is indicated by curves. The critical graph has two vertices: at one vertex three lines meet, while at the other five lines meet. Thus, the Strebel differential corresponding to this graph has one zero of order 1 and one zero of order 3.

We label the vertices of the Broom diagram to be at 0, 1, ∞, η (see Fig. 3); these correspond to the poles of the Strebel differential. The residues at these poles are given by the positive numbers p_0, p_1, p_∞, and p_η, respectively. From the figure it is easy to see that the following relations hold:

$$\begin{aligned} l_1 &= p_\infty, & l_2 + l_3 &= p_1, \\ l_4 + l_3 &= p_0, & l_4 + l_1 + l_2 &= p_\eta. \end{aligned} \tag{16}$$

Here l_1, l_2, l_3, l_4 denote the Strebel lengths of the edges of the critical graph as shown in the figure. From the above equations it is easy to solve for l_2, l_3, l_4:

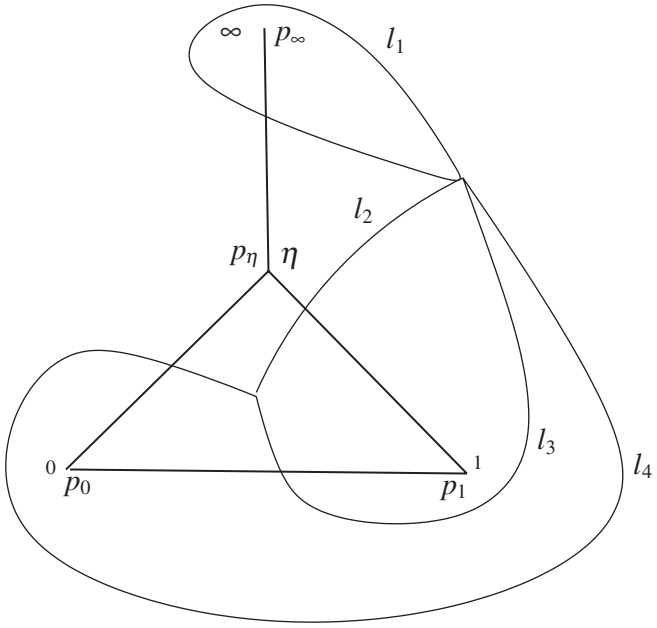

FIG. 3. The Broom diagram in field theory (the straight lines) and its dual graph.

$$l_2 = \tfrac{1}{2}(p_1 - p_0 + p_\eta - p_\infty), \tag{17}$$

$$l_3 = \tfrac{1}{2}(p_1 + p_0 - p_\eta + p_\infty), \tag{18}$$

$$l_4 = \tfrac{1}{2}(p_\eta - p_\infty - p_1 + p_0). \tag{19}$$

Thus, all the Strebel lengths are solved in terms of the residues, which indicates that in order to determine the Strebel differential of the Broom diagram for given p_i one needs to solve only algebraic equations, and not the transcendental equations involving elliptic functions in their full generality. Note also that we have focused on a particular Broom diagram, in which the vertices corresponding to 0 and 1 are connected. There are two other possible Broom diagrams (with a central vertex at η), one in which 0 and ∞ are connected and one in which 1 and ∞ are connected. All these cases are related by appropriate choices of branch cuts as mentioned in Sec. II.

Now let us look at the various limits of the Broom diagram. There are three limits (for positive p_i) and they are obtained by setting one of the edges l_2, l_3, or l_4 to zero.

$l_2 = 0$

As the edge l_2 degenerates, we see the dual edge connecting 1 and η is removed and one is left with the Π diagram in which the residues satisfy the relation

$$p_1 + p_\eta = p_0 + p_\infty. \tag{20}$$

This Π diagram, which we call the Π_1 diagram, and its dual graph are shown in Fig. 4.

$l_3 = 0$

When the edge l_3 degenerates, the Broom diagram reduces to the Y diagram in which the residues satisfy the

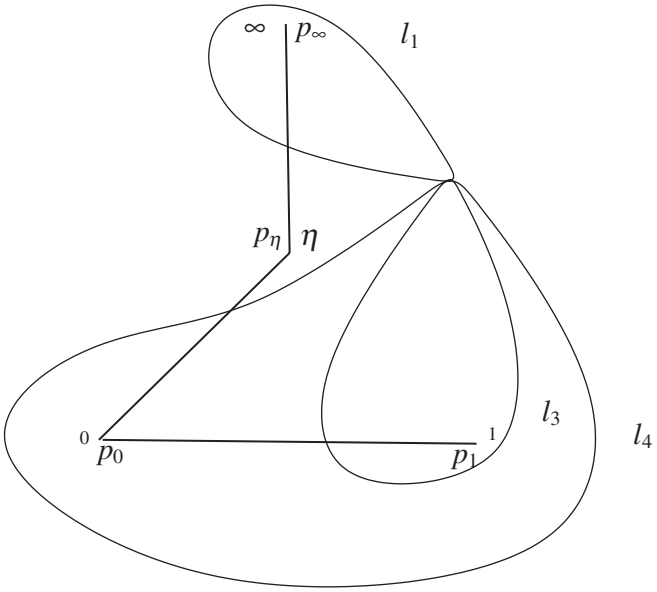

FIG. 4. The Π_1 diagram and its dual graph.

relation

$$p_0 + p_1 + p_\infty = p_\eta. \tag{21}$$

Here the dual edge joining 1 and 0 disappears, as depicted in Fig. 5.

$l_4 = 0$

In this limit, the Broom diagram reduces again to a Π diagram which is distinct from the earlier one. Here the residues satisfy the relation

$$p_\eta + p_0 = p_\infty + p_1, \tag{22}$$

and the dual edge joining η and 0 is removed, see Fig. 6. We call this diagram Π_2.

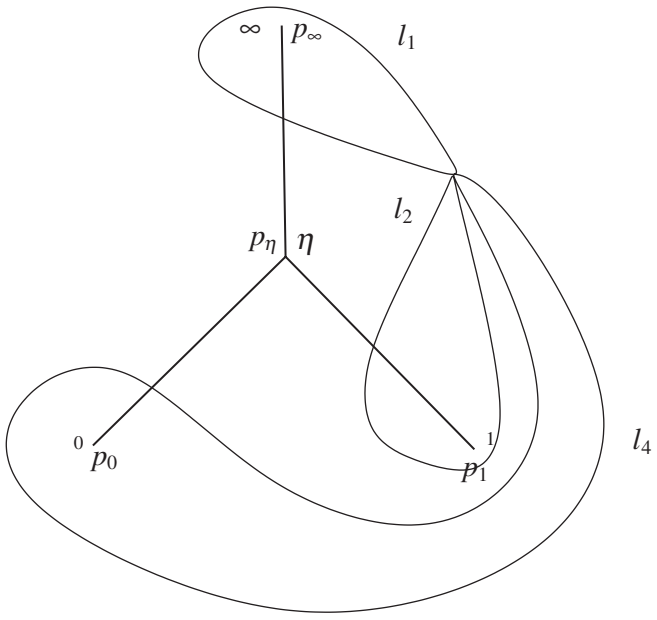

FIG. 5. The Y diagram and its dual graph.

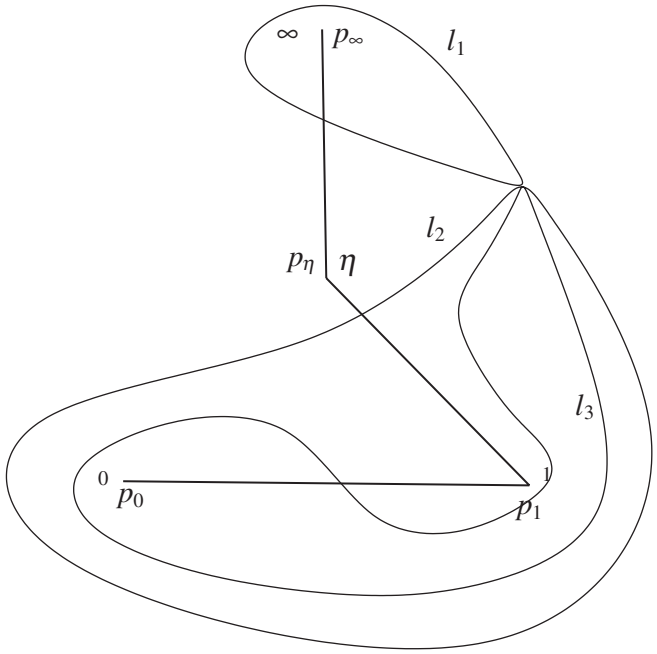

FIG. 6. The Π_2 diagram and its dual graph.

From the above discussion we see that the Π diagrams and the Y diagrams which are obtained as limits of the Broom diagram are linear subspaces in the space of the p's. In fact, since the overall scale of the Strebel differential only sets the overall scale for all lengths, we only need to consider the ratios $\frac{p_i}{p_\infty}$ $(i = \eta, 0, 1)$. Then, the Π and the Y diagrams correspond to planes in the positive octant of the three ratios.

Our goal is to compute some Broom diagrams; this should provide us with new worldsheet correlators which can be studied and lead us to a better understanding of the worldsheet CFT. Though the equations are algebraic, it is very hard to obtain closed form expressions for the cross ratio η as a function of the lengths l_i. As we will see in the next section, at a generic point in the octant of the p_i's one needs to solve a sixth order algebraic equation. Thus, closed form expressions can only be obtained on subspaces where the equations reduce to lower order ones.

We will therefore mostly use perturbation theory around the limits mentioned above. There are two different techniques to do this. One uses straightforward computations on the sphere, while the other was developed in [17] and uses expansions around special points of elliptic functions. In this section, we use the more straightforward technique, and in Appendix A we exhibit the other way to do it.[8] Of course, the final results agree precisely. As a further check we will see in the next section that the perturbation theory agrees with exact results obtained in some of the exactly solvable subspaces in a common region of intersection.

[8]It is best to read Appendix A after Sec. IV, where the relevant schemes are defined.

A. Perturbing around the Π and the *Y*

In this section we compute explicitly the first nontrivial order of the Broom diagram when expanded around the Π and *Y* diagrams. We begin with the expansion around the *Y* diagram, which exhibits many basic features of the perturbation scheme, and continue to the expansion around the Π, emphasizing the implications for the localization of the Π found in [16]. A detailed field theory analysis using the worldsheet correlator that we find is postponed to Sec. V.

1. Perturbation around the Y diagram

Let us consider the Broom diagram as a perturbation of the *Y* diagram, and write down its Strebel differential where we pick the positions of the worldsheet insertions as in Fig. 7. Our expansion around the *Y* diagram is an expansion around the subspace where the residues are related by $p_\eta = p_0 + p_1 + p_\infty$.

We scale all the Strebel lengths relative to p_∞ and define $\gamma_i = p_i/p_\infty$. The quadratic Strebel differential is

$$q dz \otimes dz = -p_\infty^2 \frac{1}{4\pi^2} \frac{(z-c)(z-c+\epsilon)^3}{z^2(z-1)^2(z-\eta)^2} dz \otimes dz. \quad (23)$$

We consider an expansion around the degenerate differential with all zeros coincident, or in other words we perform a Taylor expansion with small parameter ϵ. As mentioned above, there is no Strebel condition here, just algebraic constraints which fix the residues of the poles. The signs of the square roots of the residues γ_i^2 of (23) are set by the limit $\epsilon \to 0$ which is the *Y* diagram, for which [16] $\gamma_0 = -c^2/\eta$, $\gamma_1 = (c-1)^2/(\eta-1)$, $\gamma_\eta = (\eta-c)^2/\eta(\eta-1)$. Expanding to the first order where the constraint equation is modified we get

$$\begin{aligned}
\gamma_0 &= -\frac{c^2}{\eta} + \frac{3}{2}\frac{c}{\eta}\epsilon - \frac{3}{8}\frac{1}{\eta}\epsilon^2 - \frac{1}{16}\frac{1}{c\eta}\epsilon^3 + O(\epsilon^4), \\
\gamma_1 &= \frac{(c-1)^2}{\eta-1} - \frac{3}{2}\frac{c-1}{\eta-1}\epsilon + \frac{3}{8}\frac{1}{\eta-1}\epsilon^2 \\
&\quad + \frac{1}{16}\frac{1}{(\eta-1)(c-1)}\epsilon^3 + O(\epsilon^4), \\
\gamma_\eta &= \frac{(\eta-c)^2}{\eta(\eta-1)} + \frac{3}{2}\frac{\eta-c}{\eta(\eta-1)}\epsilon + \frac{3}{8}\frac{1}{\eta(\eta-1)}\epsilon^2 \\
&\quad - \frac{1}{16}\frac{1}{\eta(\eta-c)(\eta-1)}\epsilon^3 + O(\epsilon^4).
\end{aligned} \quad (24)$$

Let the (rescaled) length of the small edge of the Broom diagram be l (see Fig. 7):

$$2l = \gamma_0 + \gamma_1 + 1 - \gamma_\eta. \quad (25)$$

Using (24) this is equal to

$$l = \frac{1}{32}\frac{\epsilon^3}{c(\eta-c)(c-1)} + O(\epsilon^4). \quad (26)$$

Not surprisingly, the edge is nonzero only at the third order in the perturbation; the fact that the point we expand about has a fourfold degenerate zero implies that the first two contributions to the additional edge vanish. Note that in (26) one can substitute for η and c their zeroth order (in ϵ) values. The geometric meaning of this equation is very simple: it is $\frac{1}{32}\epsilon^3$ multiplied by the residue of the fourfold zero in the *Y* diagram. For all other purposes [except (26)], we may use the equations (24) to the first nontrivial order in ϵ. This should suffice to obtain the leading corrections to the amplitude written explicitly in [17]. Some trivial algebra gives the nice result:

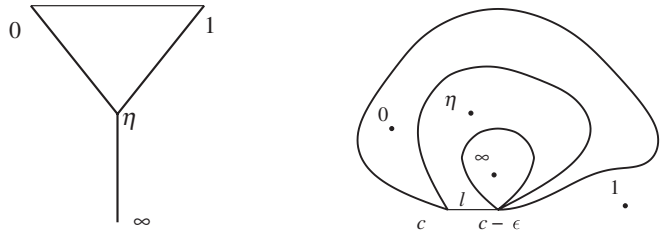

FIG. 7. The critical (and the dual) graph for the Broom expanded around the *Y* diagram.

$$c = \frac{1}{2}\left(1 + \gamma_1 - \eta(\gamma_0+\gamma_1) + \frac{3\epsilon}{2}\right) + O(\epsilon^3). \quad (27)$$

Notice that there is no correction of order ϵ^2. This will play a major role in the sequel. Substituting this in the first equation in (24) we get

$$\eta\gamma_0 = -\frac{1}{4}(1 + \gamma_1 - \eta(\gamma_0+\gamma_1))^2 + \frac{3\epsilon^2}{16} + O(\epsilon^3). \quad (28)$$

It is easy to obtain explicit formulas in the gauge we use, as was noticed in [17]. We can rewrite (28) as

$$\eta^2(\gamma_0+\gamma_1)^2 - 2\eta(\gamma_\eta\gamma_1 - \gamma_0) + (1+\gamma_1)^2 - 3\epsilon^2/4 = O(\epsilon^3), \quad (29)$$

using the relation among circumferences $\gamma_\eta = \gamma_0 + \gamma_1 + 1 + O(\epsilon^3)$. This is a quadratic equation for η, with the two solutions corresponding to two possible orientations of the *Y* diagram before the additional line is added. We choose the solution of (28) given by

$$\eta = \left(\frac{\sqrt{\gamma_\eta\gamma_1} + i\sqrt{\gamma_0}}{\gamma_0+\gamma_1}\right)^2 - \frac{3}{16}\frac{i\epsilon^2}{\sqrt{\gamma_0\gamma_1\gamma_\eta}} + O(\epsilon^3). \quad (30)$$

This is the only thing we need, in principle, for the variable change to the field theory. From here on all the equations we write will be correct up to $O(\epsilon^3)$. One can invert Eq. (30) to simplify the substitution in the field theory. First, note that

$$\eta - 1 = \left(\frac{\sqrt{\gamma_1} + i\sqrt{\gamma_\eta\gamma_0}}{\gamma_0+\gamma_1}\right)^2 - \frac{3}{16}\frac{i\epsilon^2}{\sqrt{\gamma_0\gamma_1\gamma_\eta}}. \quad (31)$$

Simple manipulations lead to the equations

$$(\gamma_0+\gamma_1)|\eta| = (1+\gamma_1) + \frac{3}{32(1+\gamma_1)}\Big[-\frac{i\epsilon^2}{\sqrt{\gamma_0\gamma_1\gamma_\eta}}(\sqrt{\gamma_\eta\gamma_1}-i\sqrt{\gamma_0})^2 + \frac{i\bar{\epsilon}^2}{\sqrt{\gamma_0\gamma_1\gamma_\eta}}(\sqrt{\gamma_\eta\gamma_1}+i\sqrt{\gamma_0})^2\Big],$$
$$(\gamma_0+\gamma_1)|\eta-1| = (1+\gamma_0) + \frac{3}{32(1+\gamma_0)}\Big[-\frac{i\epsilon^2}{\sqrt{\gamma_0\gamma_1\gamma_\eta}}(\sqrt{\gamma_1}-i\sqrt{\gamma_\eta\gamma_0})^2 + \frac{i\bar{\epsilon}^2}{\sqrt{\gamma_0\gamma_1\gamma_\eta}}(\sqrt{\gamma_1}+i\sqrt{\gamma_\eta\gamma_0})^2\Big]. \tag{32}$$

A nice consistency check is that in the zeroth order, $\epsilon = 0$, one reproduces the equations obtained in [17]. It is easy to solve the equations in the zeroth order (these are linear equations), and then to iterate and find the first correction. The zeroth order result is

$$\gamma_0 = \frac{|\eta-1|-|\eta|+1}{|\eta-1|+|\eta|-1}, \qquad \gamma_1 = \frac{|\eta|-|\eta-1|+1}{|\eta-1|+|\eta|-1}, \qquad \gamma_\eta = \frac{|\eta|+|\eta-1|+1}{|\eta-1|+|\eta|-1}. \tag{33}$$

To the end of finding the final iterated results as $\gamma = \gamma(\eta, \epsilon)$ the form (32) is not very convenient. An equivalent form of (32) (obtained by using the known zero order relations) is

$$(\gamma_0+\gamma_1)|\eta| = (1+\gamma_1) - \frac{3}{16}\frac{|\eta-1|+|\eta|-1}{|\eta|}\Big(\frac{\mathrm{Im}(\overline{\epsilon^2}\eta)}{\mathrm{Im}(\eta)}\Big),$$
$$(\gamma_0+\gamma_1)|\eta-1| = (1+\gamma_0) - \frac{3}{16}\frac{|\eta-1|+|\eta|-1}{|\eta-1|}\Big(\frac{\mathrm{Im}(\overline{\epsilon^2}(\eta-1))}{\mathrm{Im}(\eta)}\Big). \tag{34}$$

It is now trivial to solve these equations, and obtain the corrected form of the circumferences as functions of the sphere modulus η and the separation of the zeros ϵ. The first nontrivial order of the corrected solution is

$$\gamma_0 = \frac{|\eta-1|-|\eta|+1}{|\eta-1|+|\eta|-1} + \frac{3}{16}\frac{|\eta|-1}{|\eta-1|}\Big(\frac{\mathrm{Im}(\overline{\epsilon^2}(\eta-1))}{\mathrm{Im}(\eta)}\Big) - \frac{3}{16}\frac{|\eta-1|}{|\eta|}\Big(\frac{\mathrm{Im}(\overline{\epsilon^2}\eta)}{\mathrm{Im}(\eta)}\Big),$$
$$\gamma_1 = \frac{|\eta|-|\eta-1|+1}{|\eta-1|+|\eta|-1} + \frac{3}{16}\frac{|\eta-1|-1}{|\eta|}\Big(\frac{\mathrm{Im}(\overline{\epsilon^2}\eta)}{\mathrm{Im}(\eta)}\Big) - \frac{3}{16}\frac{|\eta|}{|\eta-1|}\Big(\frac{\mathrm{Im}(\overline{\epsilon^2}(\eta-1))}{\mathrm{Im}(\eta)}\Big),$$
$$\gamma_\eta = \frac{|\eta|+|\eta-1|+1}{|\eta-1|+|\eta|-1} - \frac{3}{16}\frac{1}{|\eta|}\Big(\frac{\mathrm{Im}(\overline{\epsilon^2}\eta)}{\mathrm{Im}(\eta)}\Big) - \frac{3}{16}\frac{1}{|\eta-1|}\Big(\frac{\mathrm{Im}(\overline{\epsilon^2}(\eta-1))}{\mathrm{Im}(\eta)}\Big). \tag{35}$$

Combining (26) with (24), one obtains at leading order

$$l^2 = \frac{1}{32^2}\frac{\epsilon^6}{c^2(\eta-c)^2(c-1)^2} = \frac{1}{32^2}\frac{-\epsilon^6}{\eta^2(\eta-1)^2}\frac{1}{\gamma_0\gamma_1\gamma_\eta}. \tag{36}$$

The cross ratio (30) contains ϵ^2, which means that one has to take a third root of Eq. (36). This leads to 3 possible solutions which corresponds to the 3 possible locations of the additional edge. For any value of η and l, we have three possible ways to split the zeros of the differential corresponding to Y diagram and obtain the Broom; the difference will be in the position of the extra edge. Fixing the specific diagram we want to compute uniquely fixes the branch of the cubic root as was explained in Sec. II A. We also explained in Sec. II A that the naive choice of the branch is wrong because it changes the worldsheet correlator we actually compute. This is now obvious from Eq. (36): a rotation around, say, $\eta = 0$ changes the branch upon computing the cubic root, so it would change the topology of the diagram. Note that this is consistent only if the additional edge vanishes somewhere as we do this rotation, and indeed, for $\eta \in (0, 1)$ the circumferences blow up in the zeroth order and the additional edge, consequently, vanishes.

Finally, to accomplish the variable change, we need to integrate the appropriate field theory integral (5) over the small edge, $l \equiv s_{01}$. As described in Sec. II B, we suppose that $\sum_{(i,j)\neq(0,1)} J_{ij}$ is very large compared to J_{01}. Then, this integral is dominated by a saddle point which is parametrically small $s_{01} \sim J_{01}/\sum J$. Combining with (36) we obtain that

$$\frac{J_{01}}{\sum J} \sim |\epsilon|^3, \tag{37}$$

which connects the small parameter of the expansion on the Strebel side to the small parameter in the space-time field theory.

2. *Perturbation around the* Π *diagram*

In this subsection we study the localization of diagrams on the worldsheet by perturbing around the Π diagram.[9]

[9]More specifically we work around the Π_2 diagram.

We start by discussing the relevant Strebel differential and then calculate the field theory expression. Finally, we take a short edge limit, as discussed in Sec. II B, to get an explicit worldsheet expression (our short edge is depicted in Fig. 8).[10]

For the Π diagram $p_\infty + p_1 - p_0 = p_\eta$. We begin with the differential

$$q dz \otimes dz = -p_\infty^2 \frac{1}{4\pi^2} \frac{(z-c)(z-c+\epsilon)^3}{z^2(z-1)^2(z-\eta)^2} dz \otimes dz. \quad (38)$$

ϵ is considered to be small and vanishes for the unperturbed Π diagram. As in the expansion around the Y diagram there are no reality constraints here. Expanding the residues in ϵ gives

$$\begin{aligned}
\gamma_0 &= \frac{c^2}{\eta} - \frac{3}{2}\frac{c}{\eta}\epsilon + \frac{3}{8}\frac{1}{\eta}\epsilon^2 + \frac{1}{16}\frac{1}{c\eta}\epsilon^3 + O(\epsilon^4), \\
\gamma_1 &= \frac{(c-1)^2}{\eta-1} - \frac{3}{2}\frac{c-1}{\eta-1}\epsilon + \frac{3}{8}\frac{1}{\eta-1}\epsilon^2 \\
&\quad + \frac{1}{16}\frac{1}{(\eta-1)(c-1)}\epsilon^3 + O(\epsilon^4), \\
\gamma_\eta &= \frac{(\eta-c)^2}{\eta(\eta-1)} + \frac{3}{2}\frac{\eta-c}{\eta(\eta-1)}\epsilon + \frac{3}{8}\frac{1}{\eta(\eta-1)}\epsilon^2 \\
&\quad - \frac{1}{16}\frac{1}{\eta(\eta-c)(\eta-1)}\epsilon^3 + O(\epsilon^4).
\end{aligned} \quad (39)$$

Solving for the zero and substituting back we get

$$\eta^2(\gamma_1-\gamma_0)^2 - 2\eta(\gamma_\eta\gamma_1+\gamma_0) + (1+\gamma_1)^2 - 3\epsilon^2/4 = O(\epsilon^3), \quad (40)$$

which is solved by

$$\eta = \frac{(\sqrt{\gamma_\eta\gamma_1} \pm \sqrt{\gamma_0})^2}{(\gamma_1-\gamma_0)^2} \pm \frac{3\epsilon^2}{16}\frac{1}{\sqrt{\gamma_\eta\gamma_1\gamma_0}} + O(\epsilon^3). \quad (41)$$

It is explicit that in the zeroth order the cross ratio is purely real. The sign ambiguity appearing in Eq. (41) is fixed by the choice of the ordering of insertions in the critical graph, Fig. 8 (see [16] for details). One can show that for our choice of ordering the right sign choice is $+$. Another important equation (all equations from here on are at leading nontrivial order in ϵ) is

$$2l = \gamma_\eta + \gamma_0 - \gamma_1 - 1 = -\frac{1}{16}\frac{\epsilon^3}{c(\eta-c)(c-1)}, \quad (42)$$

[10]There is another possibility of adding an extra edge to the Π diagram by making it into a Square diagram. However, also for the Square diagram the worldsheet correlator localizes on the same subspace (see Appendix B), so this does not regularize the worldsheet correlator.

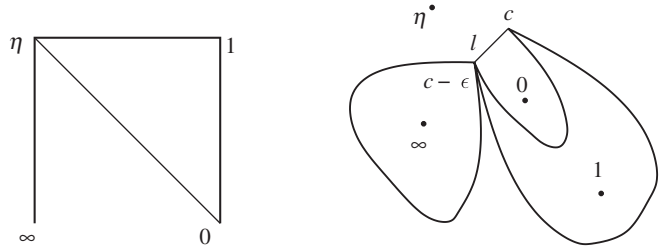

FIG. 8. The skeleton (and the dual graph) of the field theory graph we consider. The line connecting 0 and η is taken to have few contractions compared to the bold lines.

which upon using the relations above can be written in the following form:

$$l^2 = \frac{1}{32^2}\frac{\epsilon^6}{\eta^2(\eta-1)^2}\frac{1}{\gamma_0\gamma_1\gamma_\eta}. \quad (43)$$

We can put the zeroth order values of the η modulus in Eq. (43). Hence, it follows that given a specific l there are 6 solutions for ϵ, which can be written as

$$\epsilon = e^{-k\pi i/3} l^{1/3}\left[\frac{1}{32^2}\frac{1}{(\eta^{(0)})^2(\eta^{(0)}-1)^2}\frac{1}{\gamma_0\gamma_1\gamma_\eta}\right]^{-1/6}, \quad k = 0,\ldots,5, \quad (44)$$

where $\eta^{(0)}$ stands for the zeroth order solution (which is a real quantity). Recalling Eq. (41) we see that there are four deformations of the critical graph of the Π diagram for which η becomes complex and two for which it remains real at the leading order.

It is easy to see that there are indeed 6 possible blowups of the fourfold degenerate zero in the Π diagram which have a single simple zero and a threefold zero as in (38). Two of them are simply adding self-contractions to the Π which turn it into a diagram which is set to zero in the field theory. The other 4 diagrams correspond to adding a diagonal line to the Π. They come in two pairs corresponding to the mirror image of each other. In general, by imposing $l > 0$ in (42) we cut the number of diagrams to 3, and then the two complex conjugate solutions of (41) correspond to adding a diagonal line (a Broom diagram,

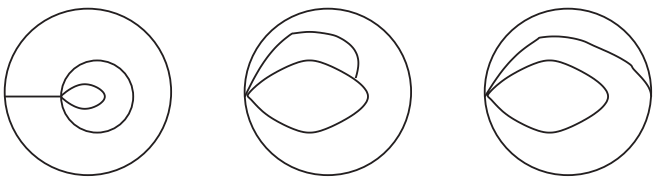

FIG. 9. Three of the 6 possible blowups of the fourfold degenerate zero, the other 3 are similar. The corresponding (dual) field theory graph contains a self-contraction for the figure on the left. The insertions are at 0, 1, η, ∞, and are exactly in this order also for the faces in the figures.

Fig. 8) and the third, real solution, corresponds to the self-contraction[11] of the vertex mapped to the point η. These deformations of the critical graph of the Strebel differential are depicted in Fig. 9.

IV. EXACTLY SOLVABLE SUBSPACES OF THE BROOM DIAGRAM

A. The Strebel differential for the Broom diagram

In this section we reanalyze the broom diagram using a different technique. This uses the uniformizing map for the Strebel differential onto an auxiliary torus. By taking appropriate scaling limits of the general case studied in [17], we can specialize to the case of the Broom diagram. We obtain a set of algebraic equations which turns out in general to be equivalent to a single sixth order equation. However, we will find subspaces where the order is lower, where we can obtain closed form expressions for the cross ratio. The techniques developed in this section will be used in Appendix A to rederive the perturbative results of the previous section and to check some of the exact results obtained here.

As mentioned above, the Strebel differential for the Broom diagram has both a third order zero and a simple zero. Therefore, it can be put in the general form

$$\phi(z)dz\otimes dz=-C\frac{(za-1)z^3}{(z-z_0)^2(z-z_1)^2(z-z_2)^2(z-z_3)^2}dz^2. \tag{45}$$

Here we have chosen the triple zero at the origin and the simple zero at $\frac{1}{a}$.[12] The equations which determine the Strebel differential for a given set of Strebel lengths are algebraic, as noted earlier. However, we will find it advantageous to work with an equivalent set of algebraic relations that one obtains from taking an appropriate limit of the general Strebel differential for a four-point function.

The most general Strebel differential can be written as

$$\phi(y)dy\otimes dy = -C'\frac{(y^2-1)(y^2k^2-1)}{(y-y_0)^2(y-y_1)^2(y-y_2)^2(y-y_3)^2}dy^2. \tag{46}$$

We substitute the change of variables

$$y=1-\epsilon^2\left(a-\frac{1}{z}\right),\qquad y_m=1-\epsilon^2\left(a-\frac{1}{z_m}\right),\qquad (m=0,1,2,3) \tag{47}$$

and take the limit $\epsilon\to 0$ with a, y, and y_m finite. We also scale C' such that C'/ϵ^{10} is finite. It easy to see that with this substitution, the general Strebel differential (46) reduces to that of the Broom diagram given in (45).

For the general Strebel differential (46), it is appropriate to go to the uniformizing variable u for the elliptic integral

$$u=\int_1^y\frac{dy}{w},\qquad w=\sqrt{(1-y^2)(1-y^2k^2)}. \tag{48}$$

To obtain the required limit we perform the substitution for y given in (47). We can then perform the integral by first expanding the integrand around the origin and then integrating term by term. This leads to the following asymptotic expansion:

$$u=-\frac{1}{\sqrt{2(k^2-1)}}\left(2\epsilon x+\frac{1-5k^2}{6(1-k^2)}(\epsilon x)^3+\frac{3+2k^2+43k^4}{80(k^2-1)}(\epsilon x)^5+\cdots\right), \tag{49}$$

where

$$x^2\equiv a-\frac{1}{z}. \tag{50}$$

From the above expansion we see that the expansion in ϵ corresponds to an expansion about $u=0$. To see this in another way, note that from the definition of u (48) we have

$$y=\frac{\mathrm{cn}(u)}{\mathrm{dn}(u)}\sim 1+\frac{1}{2}(k^2-1)u^2. \tag{51}$$

Here we have inserted the leading expansions of the functions $\mathrm{cn}(u)$ and $\mathrm{dn}(u)$ about $u=0$. Inverting the above equation we see that we obtain the leading expansion in (49).

Our goal is to determine the positions of the poles and thus their cross ratio η. The general equations for the positions of the poles in the u plane are[13]

$$\sum_{m=0}^{3}r_m\frac{1}{\mathrm{sn}(u_m)}=\sum_{m=0}^{3}r_m\,\mathrm{sn}(u_m)=\sum_{m=0}^{3}r_m\frac{\mathrm{cn}(u_m)\,\mathrm{dn}(u_m)}{\mathrm{sn}(u_m)}=0. \tag{52}$$

The r_m^2 are the residues of $\phi(z)$ at $z=z_m$, as in [17]. We can now perform an expansion in ϵ in these equations to obtain (up to order ϵ^6)

[11] This may be seen geometrically, because the original critical curve is symmetric with respect to complex conjugation. It is possible to add a self-contraction respecting this symmetry (and leaving the Strebel differential manifestly real), as in Fig. 9, while it is not possible to do this for the Broom diagram.

[12] Unlike in the general discussion and figures of the previous section, the poles are now at arbitrary positions z_i.

[13] See Eq. (2.9) in [17] and the discussion in Sec. 2 there. The location of the pole corresponding to z_m in the u-plane is denoted by u_m.

$$\sum_{m=0}^{3} r_m\left(\sqrt{2}(1-k^2)x_m + \frac{1+3k^3}{2(k^2-1)}\sqrt{(2-2k^2)}\epsilon^2 x_m^3\right) = 0,$$
$$\sum_{m=0}^{3} r_m\left(\sqrt{\frac{k^2-1}{2}}\frac{1}{x_m} + \frac{1+3k^2}{4}\sqrt{\frac{1}{2-2k^2}}x_m\epsilon^2 + \frac{(3+k^2)(5k^2-1)}{32(k^2-1)}\sqrt{\frac{1}{2-2k^2}}x_m^3\epsilon^4\right) = 0, \tag{53}$$
$$\sum_{m=0}^{3} r_m\left(\sqrt{\frac{k^2-1}{2}}\frac{1}{x_m} - \frac{3+k^2}{4}\sqrt{\frac{1}{2-2k^2}}x_m\epsilon^2 + \frac{3k^3+50k^2-5}{16(8(k^2-1))^{3/2}}x_m^3\epsilon^4\right) = 0.$$

The above equations give the following simple conditions, at leading order, for the poles:

$$\sum_{m=0}^{3} r_m x_m = \sum_{m=0}^{3} r_m \frac{1}{x_m} = \sum_{m=0}^{3} r_m x_m^3 = 0. \tag{54}$$

These equations are algebraic.

The $SL(2,\mathbb{C})$ invariant quantity which characterizes the location of the poles is their cross ratio. From the definition of x_m in (50) and its relation to the poles y_m (47) which occur in the Strebel differential, we see that the cross ratio is a function of x_m^2. Using this freedom, one can suitably change $x_m \to \pm x_m$ to write the conditions on the residues as conditions on the perimeters

$$p_0 = |r_1|, \qquad p_1 = |r_2|, \qquad p_\eta = |r_3|, \qquad p_\infty = |r_0|. \tag{55}$$

Note that all the perimeters are greater than zero. Rewriting the condition in (54) in terms of the perimeters leads to the following equations:

$$\begin{aligned} \frac{p_0}{x_1} + \frac{p_1}{x_2} + \frac{p_\eta}{x_3} &= \frac{p_\infty}{x_0}, \\ p_0 x_1 + p_1 x_2 + p_\eta x_3 &= p_\infty x_0, \\ p_0 x_1^3 + p_1 x_2^3 + p_\eta x_3^3 &= p_\infty x_0^3. \end{aligned} \tag{56}$$

In terms of the ratios

$$\gamma_i = \frac{p_0}{p_\infty}, \qquad \gamma_1 = \frac{p_1}{p_\infty}, \qquad \gamma_\eta = \frac{p_\eta}{p_\infty}, \qquad w_i = \frac{x_i}{x_0}, \qquad i = 1,2,3, \tag{57}$$

the conditions (56) reduce to

$$\frac{\gamma_0}{w_1} + \frac{\gamma_1}{w_2} + \frac{\gamma_\eta}{w_3} = 1, \qquad \gamma_0 w_1 + \gamma_1 w_2 + \gamma_\eta w_3 = 1, \qquad \gamma_0 w_1^3 + \gamma_1 w_2^3 + \gamma_\eta w_3^3 = 1. \tag{58}$$

Since the perimeters p_0, p_1, p_η, p_∞ are positive we have $\gamma_0, \gamma_1, \gamma_\eta > 0$. Thus we have to look for the solutions to the above system of equations in the $(\gamma_0, \gamma_1, \gamma_\eta)$ positive octant. These are the equations we will be using in Appendix A to analyze perturbations around some exact solutions of (58).

To make the change of variables from the Schwinger parameters to the cross ratio, we need to express the latter in terms of the Strebel lengths (which in this case are determined by the perimeters). The solutions to Eqs. (58) are sufficient to determine the cross ratio η in terms of p_0, p_1, p_η, p_∞ (or rather the ratios γ_0, γ_1, γ_η),

$$\eta = \frac{(w_3^2 - w_2^2)(w_1^2 - 1)}{(w_1^2 - w_2^2)(w_3^2 - 1)}. \tag{59}$$

Here we have used the expression for the cross ratio of the poles y_i and substituted the change of variables (47) and (50).

The equations in (58) can be reduced to a sixth order equation in one of the ratios w_i. Therefore, it is difficult to solve them in general. However, they simplify in various limits which we will discuss next.

B. Global solutions

As mentioned above, we have to look for solutions to (58) in the positive octant defined by $\gamma_0 > 0$, $\gamma_1 > 0$, $\gamma_\eta > 0$. In this octant there are three special planes in which the solutions reduce to that of the Y diagram of (21) and the Π diagrams of (20) and (22). Since these planes are important limits of the general solution, we will summarize the results for the cross ratio in these planes obtained in [16,17].

(i) *Y-plane.*—From (21) we see that the Y-plane is specified by the following linear equation in the octant:

$$\gamma_0 + \gamma_1 + \gamma_\eta = 1. \tag{60}$$

From [16,17], the formula for the cross ratio in terms of the γ's reduces to

$$\eta_{Y\pm} = \left(\frac{\sqrt{\gamma_1} \pm i\sqrt{\gamma_0\gamma_\eta}}{\gamma_0 + \gamma_1}\right)^2. \tag{61}$$

(ii) Π_1*-plane.*—We will call the subspace given by (20) the Π_1-plane

$$\gamma_1 + \gamma_\eta = 1 + \gamma_0. \tag{62}$$

The expression for the cross ratio is obtained in a way similar to the Y-plane and is given by

$$\eta_{\Pi_1\pm} = -\left(\frac{\sqrt{\gamma_0} \mp \sqrt{\gamma_1\gamma_\eta}}{\gamma_1 - \gamma_0}\right)^2. \tag{63}$$

Here we have defined $\eta_{\Pi\pm}$ corresponding to the $\mp$ branches, note that both branches are real and negative.

(iii) Π_2-*plane*.—The Π_2-plane is the subspace given by (22). In the γ-octant, its equation is given by

$$\gamma_0 + \gamma_\eta = 1 + \gamma_1. \tag{64}$$

This plane is related to the Π_1-plane by $\gamma_0 \leftrightarrow \gamma_1$ exchange. The equation for the cross ratio on this plane is given by

$$\eta_{\Pi_2\pm} = \left(\frac{\sqrt{\gamma_0} \pm \sqrt{\gamma_1\gamma_\eta}}{\gamma_1 - \gamma_0}\right)^2. \tag{65}$$

An important point to note is that the choice of branches $\eta_{Y\pm}$ is related to the choice in $\eta_{\Pi_1\pm}$ and $\eta_{\Pi_2\pm}$. We now focus on two particular limits which enable us to fix the solution globally, the diagonal line $\gamma_0 = \gamma_1 = \gamma_\eta$ and, more generally, the plane $\gamma_0 = \gamma_1$.

1. The diagonal line $\gamma_0 = \gamma_1 = \gamma_\eta = \gamma$

A nice feature of this line is that it intersects both the Π-planes,[14] (20) and (22) at $\gamma = 1$ and also the Y-plane, (21) at $\gamma = 1/3$. As we will shortly see, on this plane the equations in (58) can be exactly solved and the cross ratio can be exactly determined. In addition, matching with the solutions on the Π-planes given in (63) and (65) and the Y-plane in (61) at the intersection points will enable us to uniquely fix the branch of the solution.

We will first evaluate the cross ratio at the intersection points with the Π and the Y planes. Consider the Π_1 plane, and approach the point $\gamma = 1$ on the diagonal line along the Π_1 plane by taking $\gamma_\eta = 1 + \epsilon$, $\gamma_1 = \gamma_0 - \epsilon$. Substituting this in (63) we obtain to leading order in ϵ

$$\eta_{\Pi+} = -\frac{1}{4\gamma_0}(1 - \gamma_0)^2, \qquad \eta_{\Pi-} = -4\frac{\gamma_0}{\epsilon^2}. \tag{66}$$

The values of the cross ratio given above correspond to the two different signs in (63). We will choose the positive branch in what follows, a similar analysis can be carried out with the negative branch. What is important in our analysis is to show that the perturbation about the Π plane leads in general to a complex cross ratio; it will be easy to see that this is true in both of the branches (66). On the positive branch the value of the cross ratio at $\gamma_0 = \gamma_1 = \gamma_\eta = 1$ is given by

$$\eta_{\Pi+} = -\frac{1}{4\gamma_0}(1 - \gamma_0)^2 = 0. \tag{67}$$

Now let us look at the point $\gamma = 1/3$ where the diagonal line intersects the Y-plane. Substituting the values $\gamma_0 = \gamma_1 = \gamma_\eta = 1/3$ we obtain

$$\eta_{Y\pm} = \exp\left(\pm i\frac{\pi}{3}\right). \tag{68}$$

We again choose the positive branch here since that is what corresponds to the positive branch in the Π_1 plane. This gives the following value for the cross ratio:

$$\eta_{Y+} = \exp\left(i\frac{\pi}{3}\right) = -\omega^2, \tag{69}$$

where $\omega \equiv \exp(2\pi i/3)$ is the cube root of unity.

The Π_2 plane is related to the Π_1 plane by $\gamma_0 \leftrightarrow \gamma_1$. In fact it can be shown from (63) and (65) that $\eta_{\Pi_1\pm}(\gamma_0, \gamma_1, \gamma_\eta) = 1 - \eta_{\Pi_2\pm}(\gamma_1, \gamma_0, \gamma_\eta)$. Thus it is sufficient to focus on the Π_1 plane. Furthermore when $\gamma_0 = \gamma_1$ it seems that we have $\eta_{\Pi_1\pm}$ and $1 - \eta_{\Pi_1\pm}$ labeling the same Riemann surface. This is consistent with the $\mathbb{Z}_2$ permutation symmetry of the Broom diagram.

Let us now solve the Eqs. (58) at a general point on the diagonal line. They reduce to the following simple set of equations:

$$\frac{1}{w_1} + \frac{1}{w_2} + \frac{1}{w_3} = w_1 + w_2 + w_3 = w_1^3 + w_2^3 + w_3^3 = \frac{1}{\gamma}. \tag{70}$$

One can solve for any of the variables in the above equations to obtain the following cubic equation (we assume $\gamma \neq 1$):

$$3\gamma^2 w_3^3 - 3\gamma w_3^2 + w_3 - \gamma = 0. \tag{71}$$

Here we have chosen to eliminate w_1, w_2 and write the remaining equation for w_3. One can solve this cubic equation quite easily: under the shift $w_3 = y + \frac{1}{3\gamma}$, the equation simplifies to

$$y^3 - \frac{1}{3\gamma}\left(1 - \frac{1}{9\gamma^2}\right) = 0. \tag{72}$$

This gives the following three solutions for w_3:

$$w_3 = \frac{1}{3\gamma} + \frac{(1, \omega, \omega^2)}{3\gamma}(9\gamma^2 - 1)^{1/3}. \tag{73}$$

One can then solve for the values w_1, w_2 from the first two equations of (70).

From the symmetry of the equations in (70) it is easy to see that there are 6 solutions which correspond to the 6 permutations in the assignments of the 3 solutions in (73) to w_1, w_2, w_3. From the formula for the cross ratio in (59) one can see that a permutation involving the exchange

[14]Note, however, that this intersection point is actually a singular Π diagram where one edge is of zero length.

$(1 \leftrightarrow 2)$ has the effect $(\eta \leftrightarrow 1-\eta)$, while the exchange $(1 \leftrightarrow 3)$ has the effect $(\eta \leftrightarrow 1/\eta)$.

Since the diagonal line intersects both the Π and the Y plane at $\gamma = 1$ and $\gamma = 1/3$, respectively, we must choose the assignment such that the cross ratio reduces to the values at these points, given in (67) and (69), respectively. The following assignments satisfy this criterion uniquely:

$$w_1 = \frac{1}{3\gamma} + \frac{1}{3\gamma}\nu, \qquad w_2 = \frac{1}{3\gamma} + \frac{\omega}{3\gamma}\nu, \qquad w_3 = \frac{1}{3\gamma} + \frac{\omega^2}{3\gamma}\nu. \tag{74}$$

Here we have defined, for convenience

$$\nu \equiv (9\gamma^2 - 1)^{1/3} \tag{75}$$

to be the real value of the cube root. Evaluating the cross ratio (59) using the above assignment, we obtain

$$\eta_{\text{dia}} = -\frac{\omega^2(\nu-2)^2(\nu+1)}{(\nu-2\omega)^2(\nu+\omega)}. \tag{76}$$

It is easy to see that this expression for η vanishes at $\nu = 2$,[15] or $\gamma = 1$, which corresponds to the point where the diagonal line meets the Π-plane. It also correctly reduces to $-\omega^2$ at $\nu = 0$ or $\gamma = 1/3$, where the diagonal line meets the Y-plane.

We easily see from the exact expression (76) that, at least in the direction of this diagonal line, the cross ratio becomes complex when we perturb infinitesimally away from the Π plane(s).

2. The $\gamma_0 = \gamma_1$ plane

We will now study in a little more detail the behavior of η in the plane $\gamma_0 = \gamma_1 \equiv \gamma$. In this plane we know the exact value of η along the line $\gamma_\eta = 1$ (which is the intersection with the Π planes) as well as along the line $\gamma_\eta = \gamma$ analyzed above. We will use this exact information and study the perturbation around the Π plane and see that it is consistent with our general results.

The exact equations (58) in this plane take the simplified form

$$\frac{\gamma}{w_1} + \frac{\gamma}{w_2} + \frac{\gamma_\eta}{w_3} = \gamma(w_1 + w_2) + \gamma_\eta w_3 = \gamma(w_1^3 + w_2^3) + \gamma_\eta w_3^3 = 1. \tag{77}$$

We can eliminate w_1, w_2 from these equations and obtain a quartic equation for w_3

$$\gamma_\eta(\gamma_\eta^2 - \gamma^2)w_3^4 - \gamma_\eta^2(\gamma_\eta^2 + 3 - 4\gamma^2)w_3^3 + 3\gamma_\eta(1 + \gamma_\eta^2 - 2\gamma^2)w_3^2 - (3\gamma_\eta^2 + 1 - 4\gamma^2)w_3 + \gamma_\eta(1-\gamma^2) = 0. \tag{78}$$

In principle, it is possible to solve this quartic equation exactly and obtain the cross ratio explicitly. However, the general expressions appear to be much too cumbersome, so we will content ourselves with looking at various limits and, in Appendix A, perturbing around them.

In the limit $\gamma_\eta = 1$ we get the simple quartic equation

$$(1-\gamma^2)(w_3 - 1)^4 = 0. \tag{79}$$

For $\gamma_\eta = \gamma$, we get the cubic equation

$$w_3^3 - \frac{1}{\gamma}w_3^2 + \frac{1}{3\gamma}w_3 - \frac{1}{3\gamma} = 0, \tag{80}$$

which we had obtained and solved in the previous subsection. There is a further limit where the quartic simplifies. This is along the line $\gamma = 1$. We again get a cubic equation

$$\gamma_\eta w_3^3 - \gamma_\eta^2 w_3^2 + 3\gamma_\eta w_3 - 3 = 0. \tag{81}$$

This cubic equation can be mapped to the previous cubic in terms of the variables $w_3' = \frac{1}{w_3}$, $\gamma_\eta' = \frac{1}{\gamma_\eta}$.

V. FIELD THEORY ANALYSIS

In this section we return to the field theory and consider the worldsheet correlator for the Broom diagram, in the limit where it is close to the Π diagram. As mentioned in Sec. II, this is obtained by taking a suitable limit of a large number of contractions. We will, therefore, consider this limit in more detail.

The field theory integral, written with conductance variables as in Sec. II B, is (up to an overall numerical factor)

$$G(x_0, x_1, x_\infty, x_\eta) = \int d\sigma_{\infty\eta} d\sigma_{1\eta} d\sigma_{0\eta} d\sigma_{01} \sigma_{\infty\eta}^{m_{\infty\eta}} \sigma_{1\eta}^{m_{1\eta}} \sigma_{0\eta}^{m_{0\eta}} \times \sigma_{01}^{m_{01}} \exp[-\sigma_{\infty\eta}(x_\infty - x_\eta)^2 - \sigma_{1\eta}(x_1 - x_\eta)^2 - \sigma_{0\eta}(x_0 - x_\eta)^2 - \sigma_{01}(x_0 - x_1)^2]. \tag{82}$$

Notice that the m's are the physical multiplicities J_{ij} defined in Sec. II B minus one, and are non-negative integers. We integrate over the overall scale to get

[15] If we had chosen the negative branch in (66) we would have had to perform the $w_1 \leftrightarrow w_3$ exchange in the assignments of (76), which would have resulted in $\eta_{\text{dia}} \leftrightarrow 1/\eta_{\text{dia}}$.

$$G(x_0, x_1, x_\infty, x_\eta) = \int d\sigma_{\infty\eta} ds_{1\eta} ds_{0\eta} ds_{01} \sigma_{\infty\eta}^{m_{\infty\eta}+m_{1\eta}+m_{0\eta}+m_{01}+3} s_{1\eta}^{m_{1\eta}} s_{0\eta}^{m_{0\eta}} s_{01}^{m_{01}} \exp[-\sigma_{\infty\eta}((x_\infty - x_\eta)^2 + s_{1\eta}(x_1 - x_\eta)^2 + s_{0\eta}(x_0 - x_\eta)^2 + s_{01}(x_0 - x_1)^2)]$$
$$= \int ds_{1\eta} ds_{0\eta} ds_{01} s_{1\eta}^{m_{1\eta}} s_{0\eta}^{m_{0\eta}} s_{01}^{m_{01}} ((x_\infty - x_\eta)^2 + s_{1\eta}(x_1 - x_\eta)^2 + s_{0\eta}(x_0 - x_\eta)^2 + s_{01}(x_0 - x_1)^2)^{-M}, \tag{83}$$

where $s_i \equiv \sigma_i/\sigma_{\infty\eta}$ and $M \equiv m_{\infty\eta} + m_{1\eta} + m_{0\eta} + m_{01} + 4$. We assume that $m_{0\eta} \ll m_i$ where m_i stands for all other m's. The integration over $s_{0\eta}$ can then be performed by a saddle point approximation. Most importantly, the saddle point is dominant and the value of $s_{0\eta}$ at the saddle point is extremely small. Indeed, denoting

$$A = (x_\infty - x_\eta)^2 + s_{1\eta}(x_1 - x_\eta)^2 + s_{01}(x_1 - x_0)^2, \tag{84}$$

we have

$$s_{0\eta}|_{\text{saddle point}} = \frac{m_{0\eta}}{M} \frac{A}{(x_\eta - x_0)^2}. \tag{85}$$

Note that around the saddle point we will have an integration of the form $\int d(\delta s_{0\eta}) e^{-(1/2)\chi(\delta s_{0\eta})^2}$ with

$$\chi = \frac{M^2}{m_{0\eta}} \left[\frac{(x_\eta - x_0)^2}{A}\right]^2 = \frac{m_{0\eta}}{[s_{0\eta}|_{\text{saddle point}}]^2}, \tag{86}$$

and in order for the saddle point to be dominant χ should be very large. This is a reason why the small $m_{0\eta}$ expansion can be useful to study localization. It remains to evaluate the integral at this saddle point taking into account the quadratic fluctuations of the Gaussian. One can actually evaluate the integral exactly using the formula

$$B(x, y) = \frac{\Gamma(x)\Gamma(y)}{\Gamma(x + y)} = \int_0^\infty \frac{t^{x-1}}{(1 + t)^{x+y}} dt. \tag{87}$$

The result of the integral over $s_{0\eta}$ is given by

$$G = B(m_{0\eta} + 1, M - m_{0\eta} - 1) \int ds_{1\eta} ds_{01} s_{1\eta}^{m_{1\eta}} s_{01}^{m_{01}} ((x_\infty - x_\eta)^2 + s_{1\eta}(x_1 - x_\eta)^2 + s_{01}(x_1 - x_0)^2)^{-m_{\infty\eta}-m_{1\eta}-m_{01}-3} \times \frac{1}{(x_\eta - x_0)^{2(m_{0\eta}+1)}}. \tag{88}$$

This effectively means that we have separated out the propagators corresponding to the $m_{0\eta} + 1$ contractions, and written the others as in a Π diagram. The nontrivial input is still to come, with the transformation to the η plane. One should keep in mind that the above form of the integral would be completely useless in the case where we do not have a dominant saddle, because one cannot generally make the change of variables in the last equation [$\eta = \eta(s_{1\eta}, s_{0\eta}, s_{01})$ and $s_{0\eta}$ is generic].

We can now use our results on the Strebel problem from the previous sections to explicitly calculate the relevant worldsheet correlator, identifying the (normalized) lengths in the two formalisms, $l \sim s_{0\eta}$, $\gamma_0 \sim s_{01}$, $\gamma_1 - \gamma_0 \sim s_{1\eta}$ (in the notation of Sec. III). First, let us summarize the important relations we have established so far:

$$\epsilon^2 = e^{-(2k\pi i/3)} l^{2/3} [32^2 (\eta^{(0)})^2 (\eta^{(0)} - 1)^2 \gamma_0 \gamma_1 \gamma_\eta]^{1/3},$$
$$l|_{\text{saddle point}} = \frac{m_{0\eta}}{M} \frac{(x_\infty - x_\eta)^2 + (\gamma_1 - \gamma_0)(x_1 - x_\eta)^2 + \gamma_0 (x_1 - x_0)^2}{(x_\eta - x_0)^2}, \tag{89}$$
$$\eta = \frac{(\sqrt{\gamma_\eta \gamma_1} + \sqrt{\gamma_0})^2}{(\gamma_1 - \gamma_0)^2} + \frac{3\epsilon^2}{16} \frac{1}{\sqrt{\gamma_\eta \gamma_1 \gamma_0}}, \qquad \gamma_\eta + \gamma_0 - \gamma_1 = 1 + 2l.$$

We define $\text{Re}[\eta^{(0)}] = d^2$, to find at zeroth order in l:

$$\gamma_\eta = \frac{(d + \sqrt{\gamma_0})^2}{d^2 - 1},$$
$$\gamma_1 = \gamma_0 + \frac{(d + \sqrt{\gamma_0})^2}{d^2 - 1} - 1 = \frac{(1 + d\sqrt{\gamma_0})^2}{d^2 - 1}. \tag{90}$$

We see that d is well defined in the range $1 \le d < \infty$. In what follows we limit ourselves to small $d^2 - 1 \equiv \alpha$, since this is relevant for the OPE limit $\eta \to 1$ and it will give compact expressions. However, an analysis for general values of α is also possible.

The above relations assume smallness of ϵ and l and thus we cannot trust them for all values of the parameters.

Smallness of l implies

$$l \sim \frac{m_{0\eta}}{M}\left(\frac{x_1 - x_\eta}{x_0 - x_\eta}\right)^2 \frac{(1+\sqrt{\gamma_0})^2}{d^2-1} \ll \min(1, \gamma_0), \qquad (91)$$

which constrains γ_0 (defining $n \equiv m_{0\eta}/M$) to

$$\frac{n}{\alpha}\left(\frac{x_1 - x_\eta}{x_0 - x_\eta}\right)^2 \ll \gamma_0 \ll \frac{\alpha}{n}\left(\frac{x_1 - x_\eta}{x_0 - x_\eta}\right)^{-2}. \qquad (92)$$

For generic, finite x_i and γ_0, we see that we cannot get as close as we like to $d = 1$; we are bounded by a value of order $m_{0\eta}/M$. The smallness of l automatically implies the smallness of ϵ. Thus, we conclude that for generic x_i the calculations can be trusted for

$$n \ll \alpha \ll 1, \qquad \frac{n}{\alpha} \ll \gamma_0 \ll \frac{\alpha}{n}. \qquad (93)$$

To actually calculate the worldsheet correlator we have to establish the dictionary between the Schwinger parameters appearing on the field theory side and the cross ratio appearing in the string correlator. From (89) we find

$$\begin{aligned}\mathrm{Re}[\eta] &= d^2 - \frac{3}{2^{5/3}}\left(\frac{x_1 - x_\eta}{x_0 - x_\eta}\right)^{4/3}\frac{(1+\sqrt{\gamma_0})^{2/3}}{\gamma_0^{1/6}} n^{2/3}\alpha^{1/3},\\ \mathrm{Im}[\eta] &= \pm\frac{3^{3/2}}{2^{5/3}}\left(\frac{x_1 - x_\eta}{x_0 - x_\eta}\right)^{4/3}\frac{(1+\sqrt{\gamma_0})^{2/3}}{\gamma_0^{1/6}} n^{2/3}\alpha^{1/3}, \end{aligned} \qquad (94)$$

and we get that [define $\beta^{1/3} \equiv \frac{3^{3/2}}{2^{5/3}}(\frac{x_1 - x_\eta}{x_0 - x_\eta})^{4/3}$]

$$2^{2/3}\beta^{1/3} n^{2/3}\alpha^{1/3} < \mathrm{Im}[\eta] \ll 1 \qquad (95)$$

in the trusted regions. From (94) we can easily write down the dictionary (choosing the plus sign for $\mathrm{Im}[\eta]$):

$$\alpha = \mathrm{Re}[\eta] + \frac{1}{\sqrt{3}}\,\mathrm{Im}[\eta] - 1, \qquad (96)$$

as well as the solution for γ_0

$$\sqrt{\gamma_0^{\pm}} = \frac{\mathrm{Im}[\eta]^3}{2\beta\alpha n^2} - 1 \pm \sqrt{\frac{\mathrm{Im}[\eta]^3}{2\beta\alpha n^2}\left(\frac{\mathrm{Im}[\eta]^3}{2\beta\alpha n^2} - 2\right)}. \qquad (97)$$

The plus sign is for $\gamma_0 > 1$ and the minus sign is for $\gamma_0 < 1$. The Jacobian of the transformation $\{\mathrm{Re}[\eta], \mathrm{Im}[\eta]\} \to \{\gamma_0, d\}$ is

$$\begin{aligned}|\mathcal{J}| &= \left|2d\frac{\partial\,\mathrm{Im}[\eta]}{\partial\gamma_0}\right| \\ &= \beta n^{2/3}\alpha^{1/3}\frac{1}{3}\frac{(\sqrt{\gamma_0^{\pm}}+1)^{-1/3}(\sqrt{\gamma_0^{\pm}}-1)}{(\gamma_0^{\pm})^{7/6}}, \end{aligned} \qquad (98)$$

where we have to sum over both branches for γ_0. The Jacobian of $\{\gamma_0, \gamma_1\} \to \{\gamma_0, d\}$ is, in the vicinity of $d = 1$,

$$2\frac{(1+\sqrt{\gamma_0^{\pm}})^2}{\alpha^2}. \qquad (99)$$

From here we easily obtain that to leading order the total Jacobian is

$$6\frac{(1+\sqrt{\gamma_0^{\pm}})^{7/3}(\gamma_0^{\pm})^{7/6}}{\beta n^{2/3}\alpha^{7/3}(\sqrt{\gamma_0^{\pm}}-1)}. \qquad (100)$$

Finally, we can recast the field theory integral as a worldsheet expression. The field theory integral (88) is proportional to

$$\int d\,\mathrm{Im}[\eta]\,d\,\mathrm{Re}[\eta]\frac{(\sqrt{\gamma_0^{+}})^{1/2}}{\sqrt{\gamma_0^{+}}-1}\left(\sqrt{\gamma_0^{+}}^{m_{01}-m_{\infty\eta}} - \sqrt{\gamma_0^{+}}^{m_{\infty\eta}-m_{01}}\right)\alpha^{(2/3)+m_{\infty\eta}+m_{01}}\left(\frac{(1+\sqrt{\gamma_0^{+}})^2}{\sqrt{\gamma_0^{+}}}\right)^{-(11/6)-m_{\infty\eta}-m_{01}}. \qquad (101)$$

Here we have summed over both branches of the Jacobian. One can use the dictionary (96) and (97) to write the integrand directly in terms of the cross ratio η.

We expect that the above integrand has an extremum at the point corresponding to the unique saddle point of the field theory integral. We indeed find this maximum, which is a consistency check on the computation. The typical behavior of the integrand is shown in Fig. 10.

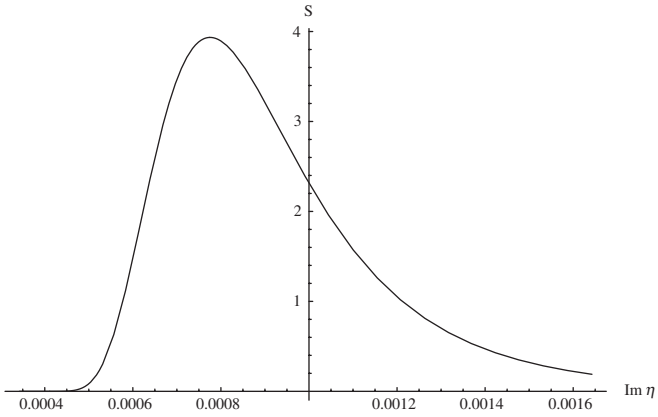

FIG. 10. A typical behavior of the integrand. Depicted here is the integrand as a function of $\mathrm{Im}[\eta]$ for some given $\mathrm{Re}[\eta]$. The vertical axis is proportional to the amplitude (denoted by S). As $m_{0\eta} \to 0$, the integrand approaches $\delta(\mathrm{Im}[\eta])$.

This provides a concrete example of our general discussion in Sec. II B; we see that in the Broom diagram the correlation function is a smooth function on the worldsheet, but that in the limit in which this diagram goes over

to the Π diagram the correlator becomes proportional to a delta function on the real line.

VI. SUMMARY AND DISCUSSION

In this paper we analyzed in detail a specific four-point function diagram, the Broom diagram, in order to illustrate several general features of the translation of [5] from Feynman diagrams to the worldsheet. We showed that this translation is modular invariant, but that the modular invariance is sometimes realized nontrivially (requiring following specific branches of fractional powers). We showed that diagrams which localize on lower-dimensional subspaces of the moduli space can be thought of as delta-function distributions, and that such a localization can be consistent with the worldsheet OPE.

While we have gained some understanding of the localization that certain worldsheet correlators exhibit, we would also like to be able to extract some broad patterns related to this behavior. For instance, we might ask the following general questions:

(i) Which free field theory diagrams exhibit localization on a subspace of the moduli space?
(ii) What subspace of the moduli space do the corresponding Strebel differentials localize on?

The idea here would be to obtain an answer to the first question based purely on the graph topology rather than through the kind of explicit computations that we have carried out. Obviously, a sufficient condition for localization (discussed in [16]) is for a diagram to have less edges than one plus the (real) dimension of the moduli space, but this is certainly not a necessary condition. An answer to the second question would also be important in studying the properties of the conjectured worldsheet theory.

So far we do not have any general answers to these questions, but we can make an observation based on the analysis of various sphere 4-point function diagrams in [16] and in this paper (including Appendix B). In these examples two types of localization occur: localization to a one-real-dimensional subspace of the two-real-dimensional moduli space, or localization to a two-dimensional region (in the Whale diagram discussed in Appendix B). In all cases, the localization is such that one of the three possible OPE limits of the diagram (which are $\eta \to 0$, $\eta \to 1$, and $\eta \to \infty$) does not appear (namely, the region covered by the Strebel map comes close to 2 of the fixed vertices but not the third one). Recall that in a 4-point function one cannot distinguish between the OPE limit of two points coming together and that of the other two points coming together (the two limits are related by a modular transformation). In all cases, we find that the worldsheet OPE limit that is not present corresponds to bringing two points together such that both pairs of the corresponding space-time operators have no contractions between them in the Feynman diagram that is being computed. For example, in the Π_1 diagram of Fig. 4, the covered region includes $\eta \to 0$ and $\eta \to \infty$ but not $\eta \to 1$, and there are indeed no contractions between the operators at η and at 1, as well as between the operators at 0 and at ∞.

We can give the following heuristic explanation for this observation. In general, the space-time OPE of single-trace vertex operators in large N gauge theories contains two types of terms (which contribute at leading order in large N to correlation functions): single-trace operators and double-trace operators. In free large N theories, the single-trace operators arise just by contractions, and they do not contribute to diagrams where there is no contraction between the two operators in the OPE. Now, in general, as discussed in [16], there is no clear relation between the space-time OPE and the worldsheet OPE in the string theory corresponding to a large N gauge theory. However, when we have an OPE between two operators in some n-point function, the single-trace terms in the space-time OPE are related to $(n-1)$-point functions, which are in turn related to $(n-1)$-point functions on the worldsheet, so it is natural to expect that the contributions related to these terms in the space-time OPE will arise from the OPE limit also on the worldsheet [which also gives $(n-1)$-point functions]. It is hard to directly relate the two OPEs because the operators appearing in the space-time OPE are non-normalizable (from the point of view of the string theory living in a higher dimensional space), and such non-normalizable single-trace operators do not appear in the worldsheet OPE;[16] however, it seems likely that some relation of this type should exist. The observation in the previous paragraph is consistent with this point of view, since the only cases where a worldsheet OPE does not exist is when it is not required to exist from the point of view of the space-time OPE. However, the observation is stronger, since one might think that a worldsheet OPE could exist even when it is not required to exist, but (in the examples that we analyzed) this does not happen. This seems to suggest that the worldsheet OPE always leads to nonzero contributions related to the single-trace operators in the space-time OPE, so that the appearance of the two is precisely correlated.

It would be interesting to check whether the observation described above can be generalized also to higher n-point functions, and whether all localizations may be explained by arguments like the one presented in the previous paragraph. It seems that more elaborate arguments are needed to explain localizations of the type found in two-point functions on the torus in [16]. It would also be interesting to understand why in some cases the diagram localizes to a lower-dimensional subspace of the moduli space, while in other localized cases it has a nonzero measure on the

[16]The question of how the worldsheet OPE is related to the space-time OPE in the AdS/CFT correspondence can be explicitly studied in the AdS_3/CFT_2 case (for some of the relevant works see [28]).

moduli space. One difference between these cases is that the localization to the lower-dimensional subspace implies strong constraints on the worldsheet OPE limit (for pairs of points which do have an OPE limit), as discussed in Sec. II C, while no such constraints arise when the localized subspace has nonzero measure. Note that when we go away from the free field theory limit we expect all of these localization properties to disappear, since at some order in the perturbation expansion in our coupling constant there should appear some diagram which covers the whole moduli space; this is consistent with the argument above, since in a nonfree theory single-trace operators in the OPE can always contribute to any correlation function, beginning at some order in the perturbation expansion.

ACKNOWLEDGMENTS

We would like to thank O. Bergman, M. Berkooz, N. Berkovits, D. Gross, N. Itzhaki, A. Neitzke, I. Yaakov, and A. Yarom for useful discussions. O. A. and Z. K. would like to thank the Institute for Advanced Study for its hospitality during the course of this project. The work of O. A. and Z. K. was supported in part by the Israel-U.S. Binational Science Foundation, by the Israel Science Foundation (Grant No. 1399/04), by the European network HPRN-CT-2000-00122, by a grant from the G.I.F., the German-Israeli Foundation for Scientific Research and Development, and by a grant of DIP (H.52). J. R. D. and R. G. are very grateful for the generous support extended to their work by the people of India. J. R. D. also thanks the string theory group at the Weizmann Institute for kind hospitality. We also thank the organizers of the Indo-Israeli meeting at Ein Boqeq where this work was initiated. The work of S. S. R. is supported in part by the Israel Science Foundation under Grant No. 568/05.

APPENDIX A: PERTURBATION EXPANSION AND THE MATCHING WITH EXACT ANSWERS

Our goal here is to find the particular branch of the perturbation expansion around the Π-plane which is consistent with the global solutions discussed in Sec. IV. We will carry out the general expansion in Appendix A 2. However, as a simpler exercise we will first perturb in the $\gamma_0 = \gamma_1 = \gamma$ plane. This will illustrate how matching with the exact solution along the diagonal line fixes the branch.

1. Perturbing around the line $\gamma_\eta = 1$

With the data of the exact solution in these limits we can study the perturbation around the line $\gamma_\eta = 1$. More precisely let us consider the strip $\gamma_\eta = 1 + \epsilon$ and fixed γ. To study the perturbation, we need to make a double expansion of (78) in ϵ and $\delta w_3 = w_3 - 1$. The resulting equation is

$$(\gamma^2 - 1)\delta w_3^4 + 8\gamma^2\epsilon\delta w_3 + 12\gamma^2\epsilon\delta w_3^2 + 4\gamma^2\epsilon^2 + 12\gamma^2\epsilon^2\delta w_3 + \cdots = 0. \quad \text{(A1)}$$

If we take $\delta w_3 \propto \epsilon^\beta$, we see that the first few terms scale as $\epsilon^{4\beta}$, $\epsilon^{\beta+1}$, $\epsilon^{2\beta+1}$, ϵ^2, $\epsilon^{2+\beta}$, respectively. It is easy to verify that we can have two consistent branches for the perturbation. In one branch $\epsilon^{\beta+1} \propto \epsilon^2$, implying $\beta = 1$. The other is where $\epsilon^{4\beta} \propto \epsilon^{\beta+1}$, which implies that $\beta = \frac{1}{3}$.

In the first expansion where $\delta w_3 \propto \epsilon$, we can show from (59) that $\eta \propto \frac{1}{\epsilon^2}$. This is not the branch we need.

In the second expansion where $\delta w_3 \propto \epsilon^{1/3}$, we find upon solving (A1) to leading order that

$$\delta w_3^3 = -\frac{8\gamma^2}{(1-\gamma^2)}\epsilon \equiv -8\mu^3\epsilon. \quad \text{(A2)}$$

Therefore, $w_1 w_2 = \frac{1-\gamma_\eta w_3}{w_3 - \gamma_\eta} w_3 = -1 + 2\mu\epsilon^{1/3}$. Here μ has to be chosen to be one of the appropriate cube roots defined by (A2), as will be fixed later. Together with the equation for $w_1 + w_2$, this gives

$$\delta w_1 = \mu\epsilon^{1/3}\frac{1-\gamma}{\gamma}, \qquad \delta w_2 = \mu\epsilon^{1/3}\frac{1+\gamma}{\gamma}. \quad \text{(A3)}$$

This gives a cross ratio (to leading order)

$$\eta = -\frac{1}{4\gamma}(1-\gamma)^2, \quad \text{(A4)}$$

which agrees with the answer obtained for the Π plane. This is, therefore, the correct branch of the perturbation expansion.

However, we see from the expression (A2) for μ that this perturbation expansion is valid away from $\gamma = 1$; it will break down in some vicinity of $\gamma = 1$. More precisely, if we take $\gamma = 1 + \delta$ for small δ, then we see from (A2) that the small parameter in the perturbation expansion is not ϵ but rather $\frac{\epsilon}{\delta} \equiv \frac{1}{b}$. We can thus approach $\gamma = 1$ as long as we choose ϵ so that $b \gg 1$.

Actually, we can independently do a perturbation expansion for arbitrary values of b. In other words consider some small neighborhood of $\gamma = \gamma_\eta = 1$. We take $\delta = b\epsilon$ and do a double expansion of (78) in δ and ϵ keeping the first few terms. We get

$$2\epsilon(w_3 - 1)[b(w_3 - 1)^3 - w_3(w_3^2 + 3)] = 0. \quad \text{(A5)}$$

Since w_3 is not identically one everywhere in this region of expansion, we have the cubic equation for w_3:

$$\alpha w_3^3 + 3w_3^2 + 3\alpha w_3 + 1 = 0, \quad \text{(A6)}$$

where $\alpha \equiv -\frac{b-1}{b}$. The roots of this cubic equation are given by

$$w_3 = \Big\{-\frac{1}{\alpha}(q+r+1), -\frac{1}{\alpha}(q\omega + r\omega^2 + 1), -\frac{1}{\alpha}(q\omega^2 + r\omega + 1)\Big\}, \tag{A7}$$

where

$$q \equiv (1-\alpha^2)^{1/3}(1+\alpha)^{1/3}, \quad r \equiv (1-\alpha^2)^{1/3}(1-\alpha)^{1/3}. \tag{A8}$$

In the $b \to \infty$ limit, we see that $q \sim 2^{1/3}/b^{2/3}$ and $r \sim 2^{2/3}/b^{1/3}$, so that to leading order in $1/b$

$$w_3 = \Big\{1 + \frac{2^{2/3}}{b^{1/3}}, 1 + \frac{2^{2/3}}{b^{1/3}}\omega^2, 1 + \frac{2^{2/3}}{b^{1/3}}\omega\Big\}. \tag{A9}$$

This exactly matches with the result of the earlier perturbation expansion (A2).

To decide which is the appropriate cube root to pick, we go back to the exact answers obtained on the line $\gamma_\eta = \gamma$. By specializing to the case $b = 1$, we restrict ourselves to this line in the vicinity of $\gamma_\eta = \gamma = 1$. In this case the possible values of w_3 from (A7) are given by

$$w_3 = \Big\{\infty, -\frac{i}{\sqrt{3}}, \frac{i}{\sqrt{3}}\Big\}. \tag{A10}$$

But from the exact answer we know that the global properties demand that we choose the middle root $w_3 = -\frac{i}{\sqrt{3}}$ [as in (74)]. Since we expect to continuously interpolate between $b = 1$ and large b, we must continue to pick the middle root in the perturbation expansion about the Π-plane in (A9) as well. As we will see in the next subsection this choice leads to the cross ratio near the Π-plane being generically complex.

2. Perturbation expansion about the Y and the Π diagrams

We now consider the perturbation expansion about a generic point in either the Π or the Y-planes. The exact global solutions discussed in the previous sections will fix the precise branch of the solution. This will enable us to show that the perturbation expansion of the cross ratio about the Π-plane is generically complex though the cross ratio on the Π-plane is real.

We first obtain a perturbation expansion either about the Y or the Π diagram by looking at a further limit of the equations in (54). From (45) we see that in the limit $a \to \infty$ we obtain the appropriate Strebel differential either for the Y or the Π diagram. Expanding the equations (54), using (50) in the $a \to \infty$ limit we obtain

$$\sum_{m=0}^{3} r_m\Big(1 - \frac{1}{2z_m a} - \frac{1}{8(z_m a)^2} - \frac{1}{16}\frac{1}{(z_m a)^3} + \cdots\Big) = 0,$$
$$\sum_{m=0}^{3} r_m\Big(1 + \frac{1}{2z_m a} + \frac{3}{8(z_m a)^2} + \frac{5}{16}\frac{1}{(z_m a)^3} + \cdots\Big) = 0,$$
$$\sum_{m=0}^{3} r_m\Big(1 - \frac{3}{2z_m a} + \frac{3}{8(z_m a)^2} + \frac{1}{16}\frac{1}{(z_m a)^3} + \cdots\Big) = 0. \tag{A11}$$

Taking linear combinations of these equations further we obtain the following equivalent set:

$$\sum_{m=0}^{3} r_m\Big(1 + \frac{1}{16}\tilde{\epsilon}^3\tilde{z}_m^3\Big) + O(\tilde{\epsilon}^4) = \sum_{m=0}^{3} r_m\Big(\tilde{z}_m + \frac{1}{8}\tilde{\epsilon}^2\tilde{z}_m^3\Big) + O(\tilde{\epsilon}^3) = \sum_{m=0}^{3} r_m\Big(\tilde{z}_m^2 + \frac{1}{2}\tilde{\epsilon}\tilde{z}_m^3\Big) + O(\tilde{\epsilon}^2) = 0, \tag{A12}$$

where $\tilde{\epsilon} = 1/a$ and $\tilde{z}_m = 1/z_m$. From these equations we see that the leading order equations reduce to those found in [17] [see Eq. (3.4)]. To solve for the corrected cross ratio to order $\tilde{\epsilon}$ we first remove the translational mode $\tilde{z}_0$ by defining $\tilde{z}_1 = \tilde{v}_1 + \tilde{z}_0$, $\tilde{z}_2 = \tilde{v}_2 + \tilde{z}_0$, $\tilde{z}_3 = \tilde{v}_3 + \tilde{z}_0$. In terms of these variables the sum of the residues in the first equation of (A12) reduces to

$$\sum_{m=0}^{3} r_m = -\frac{\tilde{\epsilon}^3}{16}(r_1\tilde{v}_1^3 + r_2\tilde{v}_2^3 + r_3\tilde{v}_3^3). \tag{A13}$$

Here we have kept terms only to $O(\tilde{\epsilon}^3)$. From this equation we see that the condition on the sum of the residues is violated only at $O(\tilde{\epsilon}^3)$. Keeping terms to $O(\tilde{\epsilon}^2)$ in the remaining two equations of (A12) we obtain

$$r_1\tilde{v}_1 + r_2\tilde{v}_2 + r_3\tilde{v}_3 = -\frac{\tilde{\epsilon}^2}{8}(r_1\tilde{v}_1^3 + r_2\tilde{v}_2^3 + r_3\tilde{v}_3^3),$$
$$r_1\tilde{v}_1^2 + r_1\tilde{v}_2^2 + r_3\tilde{v}_3^2 = -\frac{\tilde{\epsilon}}{2}(r_1\tilde{v}_1^3 + r_2\tilde{v}_2^3 + r_3\tilde{v}_3^3) + O(\tilde{\epsilon}^2). \tag{A14}$$

Note that in the last equation we have not evaluated the $O(\tilde{\epsilon}^2)$ term explicitly. We will see that this term does not contribute to the cross ratio to $O(\tilde{\epsilon}^2)$. Now define

$$v_1 = \frac{\tilde{v}_1}{\tilde{v}_3}, \qquad v_2 = \frac{\tilde{v}_2}{\tilde{v}_3}. \tag{A15}$$

Then the equations (A14) reduce to

$$r_1 v_1 + r_2 v_2 + r_3 = -\frac{\tilde{\epsilon}^2}{8}(r_1 v_1^3 + r_2 v_2^3 + r_3)\tilde{v}_3^2,$$
$$r_1 v_1^2 + r_2 v_2^2 + r_3 = -\frac{\tilde{\epsilon}}{2}(r_1 v_1^3 + r_2 v_2^3 + r_3)\tilde{v}_3 + O(\tilde{\epsilon}^2). \tag{A16}$$

It is clear from these equations that they reduce to the zeroth order equations of [17] [see Eq. (3.5)], and we need the information of $\tilde{v}_3$ at the zeroth order to solve for the first corrections in v_1, v_2. The zeroth order expression for $\tilde{v}_3$ is obtained from the deviation of the sum of perimeters. Writing (A13) in terms of v_1, v_2, and $\tilde{v}_3$ we obtain

$$-2\sum_{m=0}^{3} r_m = \frac{\tilde{\epsilon}^3}{8}(r_1 v_1^3 + r_2 v_2^3 + r_3)\tilde{v}_3^3. \tag{A17}$$

Writing $\sum_m r_m = s\tilde{\epsilon}^3$ we obtain $\tilde{v}_3$ to the zeroth order as

$$\tilde{v}_3^{(0)} = -2(1, \omega, \omega^2)\left(\frac{2s}{r_1 v_1^{(0)3} + r_2 v_2^{(0)3} + r_3}\right)^{1/3}. \tag{A18}$$

Here the superscripts in v_1 and v_2 refer to their zeroth order values. We will fix the choice of the cube root later using global considerations. Let us define

$$\delta_1 = \tfrac{1}{2}(r_1 v_1^3 + r_2 v_2^3 + r_3)\tilde{v}_3 + O(\tilde{\epsilon}),$$
$$\delta_2 = \tfrac{1}{8}(r_1 v_1^3 + r_2 v_2^3 + r_3)\tilde{v}_3^2. \tag{A19}$$

Then, the two equations of (A16) are

$$r_1 v_1 + r_2 v_2 + r_3 = -\tilde{\epsilon}^2\delta_2,$$
$$r_1 v_1^2 + r_2 v_2^2 + r_3 = -\tilde{\epsilon}\delta_1. \tag{A20}$$

We will show that the correction to the cross ratio is a function of $\tilde{\epsilon}^2\delta_1$ and $\tilde{\epsilon}^2\delta_2$, thus the $O(\tilde{\epsilon})$ correction to δ_1 in (A19) is not required at this order. Eliminating v_2 using the first equation of (A20), we obtain the following quadratic equation for v_1:

$$r_1(r_1 + r_2)v_1^2 + 2r_1(r_3 + \tilde{\epsilon}^2\delta_2)v_1 + r_3(r_3 + r_2 + 2\tilde{\epsilon}^2\delta_2) + r_2\tilde{\epsilon}\delta_1 = 0. \tag{A21}$$

Here we have retained terms to $O(\tilde{\epsilon}^2)$; note that δ_1 has an $O(\tilde{\epsilon})$ term which will not be important in the final result for the cross ratio. Solving for v_1 to $O(\tilde{\epsilon})$ we obtain

$$v_1 = \frac{-r_1(r_3 + \tilde{\epsilon}^2\delta_2) \pm \sqrt{D}}{r_1(r_1 + r_2)}, \tag{A22}$$

where

$$D = r_1 r_2 r_3 r_0 - r_1 r_2(r_1 + r_2)\tilde{\epsilon}\delta_1 - 2r_1 r_2 r_3\tilde{\epsilon}^2\delta_2. \tag{A23}$$

From the first equation of (A20) we obtain

$$v_2 = -\frac{r_2(r_3 + \tilde{\epsilon}^2\delta_2) \pm \sqrt{D}}{r_2(r_1 + r_2)}. \tag{A24}$$

The cross ratio is obtained from

$$\eta = v_1\frac{1 - v_2}{v_1 - v_2}. \tag{A25}$$

Substituting the values of v_1 and v_2 from (A22) and (A24) we obtain

$$\eta_\pm = \pm\frac{1}{(r_1 + r_2)^2\sqrt{D}}(-r_1(r_3 + \tilde{\epsilon}^2\delta_2) \pm \sqrt{D}) \times (r_2(-r_0 + \tilde{\epsilon}^2\delta_2) \pm \sqrt{D}). \tag{A26}$$

Now, expanding all terms to $O(\tilde{\epsilon}^2)$ we obtain the following expression for the cross ratio:

$$\eta_\pm = \eta_\pm^{(0)} \pm \frac{1}{\sqrt{r_1 r_2 r_3 r_0}}\tilde{\epsilon}^2\delta_2(r_1 r_2(r_0 - r_3) \pm (r_2 - r_1)\sqrt{r_1 r_2 r_3 r_0}) \pm \frac{\tilde{\epsilon}^2\delta_1^2}{4}\sqrt{\frac{r_1 r_2}{r_3 r_0}}\frac{1}{r_3 r_0}, \tag{A27}$$

where the zeroth order term for the cross ratio is given by

$$\eta_\pm^{(0)} = \pm\frac{1}{(r_1 + r_2)^2\sqrt{r_1 r_2 r_3 r_0}}(-r_1 r_3 \pm \sqrt{r_1 r_2 r_3 r_0}) \times (-r_2 r_0 \pm \sqrt{r_1 r_2 r_3 r_0}). \tag{A28}$$

Note that the corrections to the cross ratio begin at $O(\tilde{\epsilon}^2)$, and the δ_1 dependence occurs as $\tilde{\epsilon}^2\delta_1^2$. Therefore, we need only the leading term in the $\tilde{\epsilon}$ expansion of δ_1. We now have to substitute the values of δ_1 and δ_2. This is simplified by the observation

$$r_1 v_1^{(0)3} + r_2 v_2^{(0)3} + r_3 = \frac{r_3 r_0}{r_1 r_2(r_1 + r_2)^2}(r_1 r_2(r_0 - r_3) \pm \sqrt{r_1 r_2 r_3 r_0}(r_2 - r_1)). \tag{A29}$$

Using this relation one can write the term involving δ_2 in corrections to the cross ratio in (A27) in terms of δ_1^2. Then the expression for the cross ratio simplifies to

$$\eta_\pm = \eta_\pm^{(0)} \pm \frac{3}{4}\sqrt{\frac{r_1 r_2}{r_3 r_0}}\frac{1}{r_3 r_0}\delta_1^2\tilde{\epsilon}^2. \tag{A30}$$

Now, substituting the value of δ_1 from (A19) and using the relation (A29) we obtain

$$\eta_\pm = \eta_\pm^{(0)} \pm \frac{3}{16}(1, \omega^2, \omega)\frac{2^{8/3}(s\tilde{\epsilon}^3)^{2/3}}{(r_1 r_2 r_3 r_0)^{1/6}(r_1 + r_2)^{8/3}} \times (\sqrt{r_1 r_2}(r_0 - r_3) \pm \sqrt{r_3 r_0}(r_2 - r_1))^{4/3}. \tag{A31}$$

We now need to choose the value of the cube root of unity in $\tilde{v}_3^{(0)}$. We do this by systematically matching the solutions globally. Since we have chosen the positive branch of the square root we must choose the branch η_+. We fix the choice of the cube root by examining the cross ratio at the point $\gamma_0 = \gamma_1 = \gamma_\eta = 1/3 + \tilde{\epsilon}^3$. This point lies on the diagonal line, and it is also close to the Y-plane. Evaluating the cross ratio from (76) we obtain

$$\eta_{\rm dia} = -\omega^2 + i\frac{3^{13/6}}{4^{2/3}}\omega\tilde{\epsilon}^2. \tag{A32}$$

One can easily verify that it is the choice ω^2 among the roots in (A31) in which the cross ratio η_+ reduces to the above expression. Thus, the cross ratio at a generic point near the Y-plane is given by

$$\eta_{Y+} = \eta^{(0)}_{Y+} + i\frac{3}{16}\omega\frac{2^{8/3}(s\tilde{\epsilon}^3)^{2/3}}{(\gamma_0\gamma_1\gamma_\eta)^{1/6}(\gamma_0+\gamma_1)^{8/3}} \times (\sqrt{\gamma_0\gamma_1}(1+\gamma_\eta) + i\sqrt{\gamma_\eta}(\gamma_0-\gamma_1))^{4/3}, \tag{A33}$$

where $s\tilde{\epsilon}^3 = \gamma_0+\gamma_1+\gamma_\eta-1$ and $\eta^{(0)}_{Y+}$, the zeroth order cross ratio, is given in (61). Here we have made the choice $r_3=-1$, $r_2=\gamma_0$, $r_1=\gamma_1$, $r_0=\gamma_\eta$. The cross ratio at a generic point near the Π-plane is given by

$$\eta_{\Pi+} = \eta^{(0)}_{\Pi+} - \frac{3}{16}\omega^2\frac{2^{8/3}(s\tilde{\epsilon}^3)^{2/3}}{(\gamma_0\gamma_1\gamma_\eta)^{1/6}(\gamma_1-\gamma_0)^{8/3}} \times (-\sqrt{\gamma_0\gamma_1}(1+\gamma_\eta) + \sqrt{\gamma_\eta}(\gamma_0+\gamma_1))^{4/3}, \tag{A34}$$

where $s\tilde{\epsilon}^3 = 1+\gamma_1-\gamma_\eta-\gamma_0$ and $\eta^{(0)}_{\Pi+}$ is the zeroth order cross ratio given in (63). Here we have made the choice $r_1=\gamma_2$, $r_0=-\gamma_\eta$, $r_2=-\gamma_1$, $r_3=1$ to obtain the expansion about the Π_2 plane. It is clear from the above expression that the perturbation expansion of the Broom diagram about a generic point in the Π-plane leads to a complex cross ratio.

APPENDIX B: THE SQUARE AND THE WHALE DIAGRAMS

In this Appendix we discuss two additional interesting simple four-point function diagrams, the Square diagram (see Fig. 11) and the Whale diagram (see Fig. 12). Both of them obey the constraint (defining as before $\gamma_i = p_i/p_\infty$)

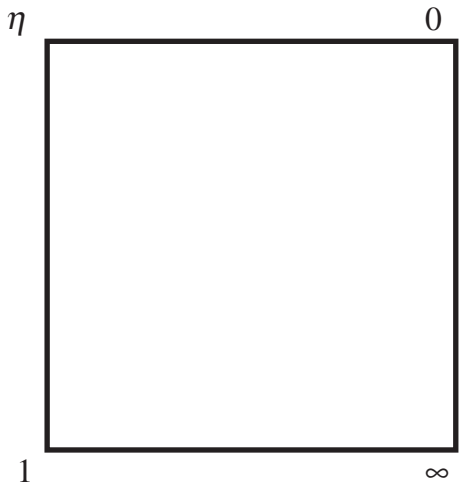

FIG. 11. The Square diagram.

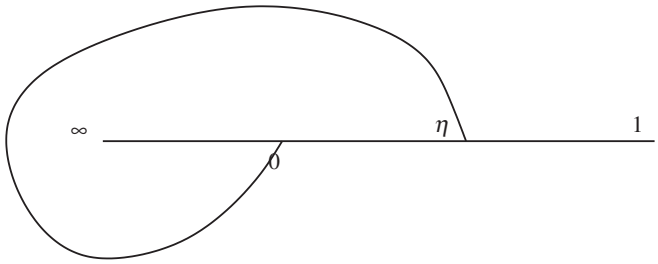

FIG. 12. The Whale diagram, which satisfies $\gamma_\eta+1=\gamma_0+\gamma_1$, like the Square diagram.

$$-\gamma_\eta+\gamma_0+\gamma_1 = 1. \tag{B1}$$

The Strebel differential is given by

$$qdz^2 = -p_\infty^2\frac{1}{4\pi^2}(d\ln F(z))^2, \qquad F(z) = z^{\gamma_0}(z-\eta)^{-\gamma_\eta}(z-1)^{\gamma_1}. \tag{B2}$$

The poles of the differential are given by poles and zeros of F (which are at 0, η, 1, and ∞). The zeros of the differential are given by the zeros of ∂F, which we will denote by $c_\pm$. We have here one Strebel condition

$$\mathrm{Re}\,[\ln F(z)]|_{c_-}^{c_+} = 0 \rightarrow FF^\dagger(c_+) = FF^\dagger(c_-). \tag{B3}$$

Next, define

$$x = -\gamma_0\eta, \qquad y = \gamma_1(1-\eta), \tag{B4}$$

so that the zeros are given by

$$2c_\pm = 1-x-y \pm \sqrt{(1+x)^2+y^2-2y(1-x)}. \tag{B5}$$

From here it is easy to see that for x, y real and $y_- \le y \le y_+$ ($x_- \le x \le x_+$), where

$$y_\pm = 1-x\pm 2\sqrt{-x} = (1\pm\sqrt{-x})^2, \qquad (x_\pm = -1-y\pm 2\sqrt{y} = -(1\mp\sqrt{y})^2), \tag{B6}$$

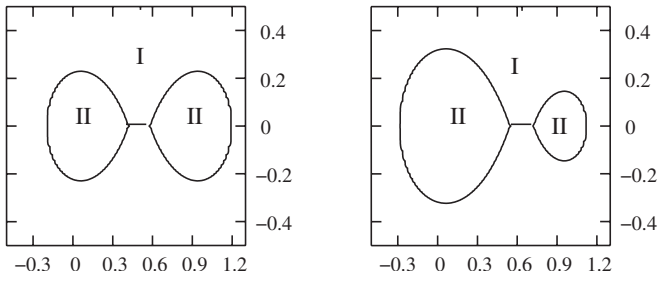

FIG. 13. The curve on the complex η plane for which the Strebel condition is satisfied. On the left $\gamma_0=\gamma_1=70$ and on the right $\gamma_0=40$, $\gamma_1=70$. In general, one can see numerically that, as γ_0 is taken to 1 the curve around $\eta=1$ shrinks to zero size, and as γ_1 is taken to 1 the curve around $\eta=0$ shrinks to zero size. This implies that the diagrams corresponding to these curves cover the full region corresponding to the OPE limits $\eta\rightarrow 0, 1$.

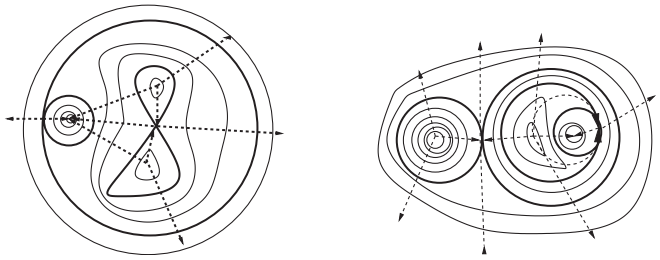

FIG. 14. The (disconnected) critical graphs and the leaves of the two possible topologies. The arrows indicate directions of increasing C. On the left we have shape I, and on the right shape II.

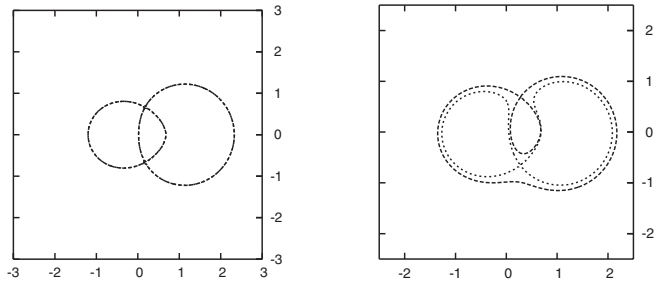

FIG. 15. On the left we draw the critical graph of the Square diagram for a typical real solution. On the right we have the critical curves when slightly moving to the complex plane. We see how the graph smoothly becomes disconnected, and has topology I.

the reality condition (B3) is satisfied as the two zeros are complex conjugates of each other. Note that the zeros can be rewritten as

$$c_\pm = \left(\frac{\sqrt{y_+ - y} \pm \sqrt{y_- - y}}{2}\right)^2, \qquad c_\pm - 1 = \left(\frac{\sqrt{x_+ - x} \mp \sqrt{x_- - x}}{2}\right)^2. \tag{B7}$$

Further, the dictionary between the two sets of variables is given by

$$\eta = \frac{x(y-\bar{y})}{y\bar{x} - x\bar{y}}, \qquad \gamma_0 = \frac{x\bar{y} - \bar{x}y}{y - \bar{y}}, \qquad \gamma_1 = \frac{x\bar{y} - \bar{x}y}{x - \bar{x}}. \tag{B8}$$

Note that when η is real the transformation is singular, but as we saw above in this case we can solve the Strebel problem.

From Eq. (B3) we see that there is no solution for large η's. Note that when we take η to be large and at least one of the circumferences does not scale to zero, one of the zeros $c_\pm$ becomes large and the other remains finite, and the condition (B3) cannot be satisfied. Recall that γ_0 and γ_1 cannot both be small due to (B1). The fact that there are no solutions for large η means that the OPE of the vertices at η and at ∞ is not covered by diagrams satisfying (B1). The solution of Eq. (B3) can be obtained numerically, and has the general shape depicted in Fig. 13.

The nice feature of the Strebel differential (B2) is that the horizontal leaves can be computed here explicitly. The horizontal leaves satisfy

$$\left(\frac{dz}{dt}\right)^2 > 0, \tag{B9}$$

and thus

$$\frac{d}{dt}\,\mathrm{Re}[\ln F(z)] = 0 \rightarrow F(z(t))F^\dagger(\bar{z}(t)) = C. \tag{B10}$$

Here C is a non-negative constant parametrizing a certain leaf. The Strebel condition (B3) now has a nice interpretation: the C parameter for both zeros has to be equal, and this is required if we want a leaf to go from one zero to another. Otherwise, either the leaves emanating from a zero will not be compact (will not end) or they will end on the same zero and the critical graph will be disconnected. Both of these cases contradict the Strebel conditions.

We still have to identify which diagram the various solutions depicted in Fig. 13 correspond to. The only two diagrams which have the Strebel differential (B2) are the Square diagram and the Whale diagram.

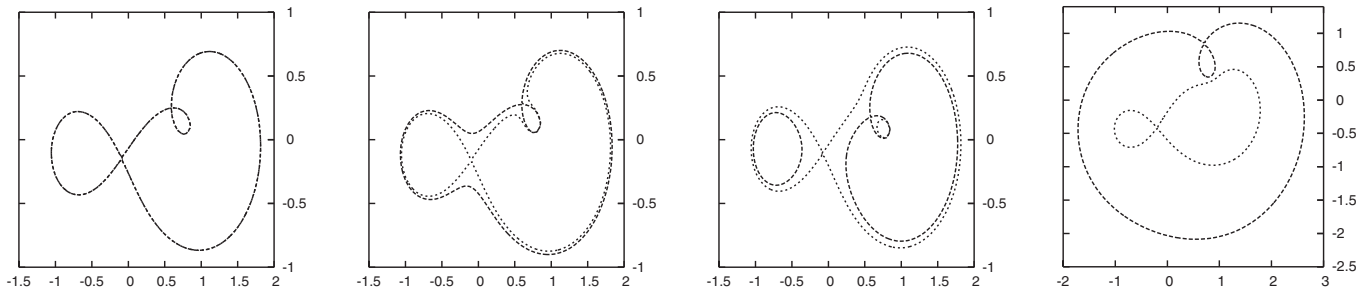

FIG. 16. On the left, we draw the critical graph of a complex solution for η. It is easy to see that this critical graph is dual to the Whale diagram. In the next two graphs we again slightly move away from the point where the Strebel conditions are satisfied. We keep the same real part of η and first move up and then down along the imaginary axis. The critical graph has topology II when lowering $\mathrm{Im}(\eta)$, and topology I when raising $\mathrm{Im}(\eta)$. The last graph is a generic complex η not satisfying the Strebel conditions. The critical graph is disconnected and we do not have a cell decomposition.

We claim that the solution corresponding to the Square is the real[17] η solution on the straight line in Fig. 13, and the other solutions correspond to the Whale. First, note that at a generic point of the η plane (where the Strebel condition is not satisfied) the horizontal leaves begin and end on the same zero, and can have only two topologically distinct shapes. This follows from the fact that the nodes of the graph (the zeros of the Strebel differential) correspond to saddle points of $FF^\dagger$ (as the zeros are second order), and from the fact that the parameter C goes to zero in the vicinity of 0 and 1 and diverges as one approaches ∞ or η. We can call the two shapes shape I and shape II, see Fig. 14. It is easy to show that the graph in Fig. 13 is the boundary region between the two different shapes. The real line is the boundary between two different ways to get shape I, and the complex solution is the boundary between shape I and II. When one goes between the two ways to get shape I, one gets a dual of a Square diagram, and when going from I to II one obtains the dual of the Whale diagram. The topology in the different regions is shown in Fig. 13.

In Figs. 15 and 16, we depict the critical graphs of the Square, the Whale, and the additional diagrams that we get by slightly deforming away from the solution to the Strebel condition (B3).

[16]Note that these real solutions span only the interval $\eta \in (0, 1)$, and thus the cross ratio of the square can take values only in this interval.

[1] G. 't Hooft, Nucl. Phys. **B72**, 461 (1974).
[2] R. Gopakumar and C. Vafa, Adv. Theor. Math. Phys. **3**, 1415 (1999); H. Ooguri and C. Vafa, Nucl. Phys. **B641**, 3 (2002).
[3] E. Witten, Surveys Diff. Geom. **1**, 243 (1991); M. Kontsevich, Commun. Math. Phys. **147**, 1 (1992); D. Gaiotto and L. Rastelli, J. High Energy Phys. 07 (2005) 053.
[4] J. M. Maldacena, Adv. Theor. Math. Phys. **2**, 231 (1998); Int. J. Theor. Phys. **38**, 1113 (1999); S. S. Gubser, I. R. Klebanov, and A. M. Polyakov, Phys. Lett. B **428**, 105 (1998); E. Witten, Adv. Theor. Math. Phys. **2**, 253 (1998).
[5] R. Gopakumar, Phys. Rev. D **70**, 025009 (2004); **70**, 025010 (2004); C.R. Physique **5**, 1111 (2004); Phys. Rev. D **72**, 066008 (2005).
[6] K. Bardakci and C. B. Thorn, Nucl. Phys. **B626**, 287 (2002); C. B. Thorn, Nucl. Phys. **B637**, 272 (2002); **B648**, 457(E) (2003); K. Bardakci and C. B. Thorn, Nucl. Phys. **B652**, 196 (2003); S. Gudmundsson, C. B. Thorn, and T. A. Tran, Nucl. Phys. **B649**, 3 (2003); K. Bardakci and C. B. Thorn, Nucl. Phys. **B661**, 235 (2003); C. B. Thorn and T. A. Tran, Nucl. Phys. **B677**, 289 (2004); K. Bardakci, Nucl. Phys. **B715**, 141 (2005); M. Kruczenski, J. High Energy Phys. 10 (2006) 085; K. Bardakci, arXiv:hep-th/0701098.
[7] P. Haggi-Mani and B. Sundborg, J. High Energy Phys. 04 (2000) 031; H. L. Verlinde, J. High Energy Phys. 12 (2003) 052; J. G. Zhou, Phys. Rev. D **67**, 026010 (2003); D. Vaman and H. L. Verlinde, J. High Energy Phys. 11 (2003) 041; A. Dhar, G. Mandal, and S. R. Wadia, arXiv:hep-th/0304062; K. Okuyama and L. S. Tseng, J. High Energy Phys. 08 (2004) 055; L. F. Alday, J. R. David, E. Gava, and K. S. Narain, J. High Energy Phys. 09 (2005) 070; J. Engquist and P. Sundell, Nucl. Phys. **B752**, 206 (2006); L. F. Alday, J. R. David, E. Gava, and K. S. Narain, J. High Energy Phys. 04 (2006) 014.
[8] J. Polchinski (unpublished).
[9] A. Karch, arXiv:hep-th/0212041; A. Clark, A. Karch, P. Kovtun, and D. Yamada, Phys. Rev. D **68**, 066011 (2003).
[10] G. Bonelli, J. High Energy Phys. 11 (2004) 059.
[11] N. Itzhaki and J. McGreevy, Phys. Rev. D **71**, 025003 (2005).
[12] M. Bianchi, J. F. Morales, and H. Samtleben, J. High Energy Phys. 07 (2003) 062; N. Beisert, M. Bianchi, J. F. Morales, and H. Samtleben, J. High Energy Phys. 02 (2004) 001; D. E. Diaz and H. Dorn, J. High Energy Phys. 07 (2006) 022.
[13] E. T. Akhmedov, Pis'ma Zh. Eksp. Teor. Fiz. **80**, 247 (2004) [JETP Lett. **80**, 218 (2004)].
[14] M. Carfora, C. Dappiaggi, and V. L. Gili, J. High Energy Phys. 12 (2006) 017; arXiv:hep-th/0702114.
[15] K. Furuuchi, Phys. Rev. D **72**, 066009 (2005).
[16] O. Aharony, Z. Komargodski, and S. S. Razamat, J. High Energy Phys. 05 (2006) 016.
[17] J. R. David and R. Gopakumar, J. High Energy Phys. 01 (2007) 063.
[18] I. Yaakov, J. High Energy Phys. 11 (2006) 065.
[19] K. Strebel, *Quadratic Differentials* (Springer-Verlag, Berlin, 1984).
[20] M. Mulase and M. Penkava, arXiv:math-ph/9811024.
[21] D. Zvonkine, arXiv:math.AG/0209071.
[22] B. Zwiebach, Nucl. Phys. **B390**, 33 (1993); A. Belopolsky and B. Zwiebach, Nucl. Phys. **B442**, 494 (1995).
[23] N. Moeller, J. High Energy Phys. 11 (2004) 018; J. High Energy Phys. 03 (2007) 043.
[24] S. K. Ashok, F. Cachazo, and E. Dell'Aquila, arXiv:hep-th/0610080.
[25] D. J. Gross and P. F. Mende, Phys. Lett. B **197**, 129 (1987); Nucl. Phys. **B303**, 407 (1988).
[26] E. Witten, Commun. Math. Phys. **252**, 189 (2004); N. Berkovits, Phys. Rev. Lett. **93**, 011601 (2004).
[27] R. C. Brower, J. Polchinski, M. J. Strassler, and C. I. Tan, arXiv:hep-th/0603115.
[28] J. M. Maldacena and H. Ooguri, Phys. Rev. D **65**, 106006 (2002); J. R. David, G. Mandal, and S. R. Wadia, Phys. Rep. **369**, 549 (2002); M. R. Gaberdiel and I. Kirsch, arXiv:hep-th/0703001; A. Dabholkar and A. Pakman, arXiv:hep-th/0703022.